Toward quantifying geomorphic rates of crustal displacement, landscape development, and the age of glaciation in the Venezuelan Andes

Steven G. Wesnousky[a], Reina Aranguren[b], Martin Rengifo[b], Lewis A. Owen[c], Marc W. Caffee[d], Madhav Krishna Murari[c], and Omar J. Pérez[e]

[a] Center for Neotectonic Studies, University of Nevada, Reno, NV 89557, USA.
[b] Laboratorio de Geofísica, Universidad de Los Andes, Mérida, Venezuela.
[c] Department of Geology, University of Cincinnati, Cincinnati, OH 45221, USA
[d] Department of Physics, PRIME Laboratory, Purdue University, Lafayette, IN 47906, USA
[e] Department of Earth Sciences, Universidad de Simón Bolivar, Caracas, Venezuela

Abstract

We present the results of dating glacial landforms in Venezuela using 10Be terrestrial cosmogenic nuclide (TCN) analysis and optical stimulated luminescence (OSL). Boulders on the La Victoria and Los Zerpa moraines of the Sierra Nevada that mark the extent of the local last glacial maximum (LLGM) yield 10Be TCN surface exposure ages of 16.7 ± 1.4 ka (8 samples). About 25 km to the west in the drainage basin of the Río Mucujún, ^{10}Be TCN dates for boulders on moraines at La Culata in the Sierra Nevada Norte yield a younger average age of 15.2 ± 0.9 ka (8 samples). The data suggest that glaciation across the Venezuelan Andes during the LLGM was asynchronous. The LLGM in Venezuela may be broadly concurrent with Heinrich Event 1 at ~ 16.8 ka, implying that glaciation here is dominantly temperature driven. A moraine inset into the older laterofrontal moraines of La Culata has an age of 14.1 ± 1.0 mm (5 samples); it may have been deposited by a small Late Glacial readvance. Right-lateral offsets of the La Victoria and Los Zerpa moraines by the Boconó fault are each ~ 100 m. The ^{10}Be TCN based Boconó fault slip rate is about < ~5.5 to 6.5 mm a^{-1}, notably less than the total right-lateral slip of 12 ± 2 mm a^{-1} of shear documented across the Andes from geodesy. The ^{10}Be TCN dating of boulders on a faulted alluvial fan along the northwestern rangefront at Tucanízón yields a late Pleistocene uplift rate of the Andes at between ~ 1.7 ± 0.7 mm a^{-1}. Glacial outwash has produced valley-fill sequences within the central Andean valley along the trace of the Boconó fault and Río Chama. Here, fill has been incised to produce the 'meseta,' a terrace surface that sits > 100 m above the Río Chama and on which the major city of Mérida is built. Geomorphic observations indicate that the meseta deposits were largely derived from the glaciers of La Culata. The OSL dating suggests that the final aggradation of the valley-fill deposits occurred rapidly over a period of about 5 to 6 ka and that the surface was abandoned and initially incised at ~ 30 ka. The result implies Venezuelan valley fills record phases of aggradation that are likely modulated by climate change on glacial/Milankovitch timescales.

Keywords: Venezuelan Andes; terrestrial cosmogenic nuclides; optically stimulated luminescence; glaciation; moraines; alluvial fans; active fault; slip-rates

1. Introduction

The Venezuelan Andes sit at the equatorial latitude of ~ 8° N, reach elevations of ~ 5000 m above sea level (asl), and archive successions of well-preserved glacial, fluvial, and mass movement landforms and sediments (Figs. 1 and 2). Uplift of the Venezuelan Andes is a

response to transpression along the southern Caribbean transform plate boundary. The uplift and transpression are recorded in displacements of the Boconó strike-slip fault system that runs along strike and within the Andean range and in the thrust faults that delimit the rangefronts. Throughout the Quaternary, glaciers and associated river systems have eroded deep valleys across the mountain range, through which abundant sediment was transferred to the equatorial forelands.

The Venezuelan Andes are one of a few equatorial regions where glacial successions are present and well-preserved (e.g., Thackray et al., 2008). Large laterofrontal moraines are present in many of the valleys (e.g., Schubert, 1998). Dating of these landforms and associated sediments yields paleoclimatic records (e.g., Stansell et al., 2005). Many of the moraines and terraces are offset by the Boconó fault and the associated flanking thrust faults, and therefore also preserve a record of horizontal and vertical crustal displacement rates (e.g., Schubert and Sifontes, 1970). Detailed data on fault-slip rates are ultimately needed to develop models for landscape evolution and to evaluate seismic hazard.

As a significant step toward quantifying rates of landscape evolution, testing, and refining glacial chronologies, and determining rates of crustal displacement, we have (i) used ^{10}Be terrestrial cosmogenic nuclide (TCN) surface exposure analysis to date several large laterofrontal moraines that are either near or displaced by the Boconó fault and an alluvial fan surface that is displaced by the thrust fault bounding the northwest flank of the Andes and (ii) used optically stimulated luminescence (OSL) to date glacial outwash deposits that filled the central Andean valley that follows the Boconó fault near the city of Mérida. The selected large laterofrontal moraines also mark the maximum glacier extent during the last glacial.

We begin with a brief description of the physiographic, climatic, and plate tectonic setting and then describe the methods used to determine the ages of the landforms and sediment. Descriptions of the respective study areas and our findings follow. The new observations are then discussed in the context of prior work that bears on the glacial history, neotectonics, and geodesy of the Venezuelan Andes.

2. Regional setting

The Venezuelan Andes are ~ 100 km wide and extend for ~ 450 km across northern Venezuela from the Colombian border in the southwest to Barquisimeto in the northeast. Northern Venezuela sits astride the boundary between the Caribbean and South American tectonic plates (Fig**.** 1). The tectonic structure of northern Venezuela is a consequence of the relative plate motion between the South American and Caribbean plates (e.g., Sykes et al., 1982). The Caribbean plate moves eastward relative to the South American plate at a rate of ~ 18 mm a^{-1}. (DeMets et al., 2010). The Boconó and El Pilar fault systems mark the southern boundary of the Caribbean plate (Pérez and Aggarwal, 1981). The El Pilar system strikes east-west and is characterized by pure right-lateral strike-slip motion (e.g., Pérez, 1998). The Boconó fault runs largely along the axis of the Venezuelan Andes (Fig**.** 2), which is oriented obliquely to the relative plate motion vector between the Caribbean and South American plates (Fig. 1). The plate motion is partitioned between pure strike-slip along the Boconó and thrusting along the margins of the Venezuelan Andes and also the Caribbean coast to the north (Figs. 1 and 2; e.g., Pérez et al., 1997). Estimates of cumulative right-offset along the Boconó fault system are quite varied (Schubert, 1982) and range upward to ~ 150 km (Pindell et al., 1998).

Unlike the major portion of the Andes that strikes along the west flank of South America, the Venezuelan Andes are devoid of volcanoes and the uplift of the Andes may be attributed solely to tectonics or, more specifically, thrust faulting and folding along the margins of the range (e.g., Audemard and Audemard, 2002).

The climate of the region is tropical with one rainy season. The north-south precipitation gradient is broad with the northern slopes of the Venezuelan Andes receiving less rainfall than the southern slopes. The topographic controls on climate are strong throughout the region. The annual rainfall in the mountains is generally around 1000 mm. In contrast, the plains, for example, around Lago de Maracaibo receive ~ 580 mm of rainfall annually and the temperature is hot all year; typical daily average maximum temperatures are in the mid-30s °C. In the Llanos region south of the Andes, the annual average rainfall is 1500 mm, temperatures are likewise in the mid-30s °C all year, and there is persistent high humidity (Meteorological.Office, 2011).

Elevations in the central Andes consistently peak in excess of 3500 m asl (Fig**.** 2). This is also the approximate lower limit of the maximum extent of glaciers during the last glacial, locally referred to as the Mérida glaciation (Schubert, 1974; Stansell et al., 2007b). The maximum area covered by glaciers during the last glacial was about 600 km^2 (Schubert, 1998). The Boconó fault and the linear valley that is commonly aligned along its length divide these regions of high elevation and glaciation (Fig**.** 2). The high Andes to the north of the Boconó are referred to as the Sierra Norte and those to the southwest of the Boconó as the Sierra Nevada (Fig**.** 2). The northeasternmost extent of the glaciated Sierra Nevada is also referred to as the Sierra de Santo Domingo. Locally, the Sierra Norte is often referred to as the Sierra de Culata. More than 70 peaks in the region record elevations > 4300 m asl (León, 2001). The number and size of remnant glaciers diminished rapidly during the last ~ 150 years (Schubert, 1998 ; and references therein). Annual snowfall is recorded only on three of the highest peaks (Pico Bolívar, 4981 m asl; Pico Humboldt, 4940 m asl; and Pico Bonpland, 4883 m asl; Jahn, 1912; Pérez et al., 2005). These peaks support five cirque glaciers that today cover an area of only ~ 2 km^2 (Stansell et al., 2007b).

3. Methods

3.1. Mapping

Our study commenced with construction of a strip map documenting the location and type of offset Quaternary landforms along the Boconó fault and placing the Boconó fault in the context of the distribution of Quaternary basins and sediments along the fault zone. The same approach was also taken along several stretches of the Andean rangefronts. The mapping was conducted with aerial photographs ranging in scale from 1:25,000 to 1:40,000 and field observation. Several of the figures in this paper are extracted from our map**.**

3.2. Numerical dating

We used ^{10}Be TCN dating of surface boulders (Gosse and Phillips, 2001, and references therein) and OSL (optically stimulated luminescence) dating of sediment to obtain age estimates for moraines surfaces, alluvial fans/terraces, and valley-fill sediments. Samples were collected from surface boulders composed of quartz-rich gneiss for ^{10}Be TCN dating. Large boulders (> 1 m ~high) were preferentially sampled from sites that showed none or minimal surface erosion. Boulders were sampled from crests of moraines; on the alluvial fans/terraces, boulders were collected on high surfaces away from channels. Approximately 500 g of rock was chiseled off

the upper ≤ 5 cm surface. The location, rock type, and size of each sample were recorded and photographed. These are listed in Table 1. The inclination from the sampled surface to the surrounding horizon was measured to quantify topographic shielding.

Boulder samples were prepared at the Quaternary Geochronology Laboratories at the University of Cincinnati. Samples were crushed and sieved to obtain a 250-500 μm grain size fraction. The 250-500 μm size fraction was processed using four acid leaches: aqua regia for > 9 h, two 5% HF/HNO_3 leaches for ~ 24 h, and one 1% HF/HNO_3 leach for 24 h. Lithium heteropolytungstate heavy liquid separation was applied after the first 5% HF/HNO_3 leach. Atomic absorption spectrometry (AAS) Be carrier was added to the pure quartz. The quartz was dissolved in 49% HF and HNO_3 and passed through anion and cation exchange columns along with chemical blanks to extract $Be(OH)_2$. The $Be(OH)_2$ was oxidized to BeO through ignition at 750°C and mixed with Nb powder and loaded in stainless steel targets for the measurement of the $^{10}Be/^{9}Be$ ratios by accelerator mass spectrometry (AMS). AMS measurements were made at the PRIME Laboratory in Purdue University. Details for standards, blanks, age calculations are shown in the footnotes of Table 1.

The ^{10}Be TCN ages we report do not correct for erosion and thus place a minimum limit on the age of exposure (Table 1). The appropriate scaling models and geomagnetic corrections for TCN production to calculate TCN ages is a topic of debate (e.g., Pigati and Lifton, 2004; Staiger et al., 2007; Balco et al., 2008); we used the constant (time-invariant) local production based on Lal (1991) and Stone (2000). The spread between exposure ages using different scaling models for the latitude and altitudes of our study areas is between 5-16% for samples that date between 11 and 21 ka, 11-21% for samples that date between 40 and 100 ka, and up to 19% for samples older than 100 ka (Table 1).

The TCN ages on Quaternary surfaces are affected by several geological factors. Weathering, exhumation, prior exposure, and shielding of the surface by sediment and/or snow will generally produce an underestimate of the true age of the landforms (Owen et al., 2011a,b). In contrast, exposure of rock surfaces prior to deposition on the landform being dated results in overestimates of true ages of the landform.

The stochastic nature of geological processes can produce a large spread in apparent exposure ages on a landform. Collecting multiple samples on a surface provides a measure of these effects. If similar apparent ages are found for multiple surface samples, it may be inferred that the dated samples were not derived from older surfaces, exhumed at different times from the subsurface subsequent to deposition, or subject to different rates of degradation since deposition on the surface. Accordingly, the TCN dates are at worst minimum ages and at best they are the actual age of the landform. Putkonen and Swanson (2003) and Heyman et al. (2011) argue that prior exposure is rare on moraines and that erosion of the landform and the boulder itself is more common; such that the oldest date in a population of TCN dates on a surface more likely reflects the true age of the landform. Boulders with prior exposure are more common on alluvial fans and terraces (e.g., Owen et al., 2011a,b) and younger ages in the population of TCN dates might be closer to the true age of the landforms. Determining which date(s) in a population most closely represents the true age of the landform is thus uncertain. In this paper, we quote the mean of all ages for each particular surface and use the standard deviation as a measure of the uncertainty. The generally tight clustering of ^{10}Be TCN dates obtained for moraine surfaces in this study

provides a good degree of confidence that our ^{10}Be TCN ages closely represent the actual ages of the moraines.

The OSL methodology is applied to several samples collected from stratigraphic levels of valley-fill deposits. The technique measures the time since quartz and feldspar were last exposed to sunlight and therefore the deposition and burial of a particular sedimentary level. A comprehensive review of the methods is presented in Aitken (1998).

Samples for OSL dating were obtained by hammering opaque plastic tubes, ~ 20 cm - long, into fresh, natural exposures. The tubes were sealed and placed in light-proof photographic bags until the initial processing at the University of Cincinnati. Laboratory preparation follows the methods described in Seong et al. (2007). The luminescence signals were measured using a Riso TL/OSL reader (model DA-20). Luminescence from the quartz grains was stimulated using an array of blue-light-emitting diodes (470 nm, 50 mW cm^{-2}) filtered using a green long-pass GG-420 filter; detection was through a Hoya U-340 filter. All quartz aliquots were screened for feldspar contamination using infrared stimulation with infrared-light-emitting diodes (870 nm, 150 mW cm^{-2}). All OSL signals were measured using a 52-mm-diameter photomultiplier tube (9235B). The equivalent dose (D_E) measurements were determined on multiple aliquots using the single aliquot regenerative (SAR) method protocol developed by Murray and Wintle (2000). Growth curve data were fitted using linear and exponential trend curves. The D_E value for every aliquot was examined using Riso Analysis 3.22b software. Aliquots with poor recuperation (> 10%) were not used in the age calculations. Equivalent doses of all aliquots were averaged for each sample then divided by the dose rate giving a mean age (Table 2). Calculation uncertainties and methods used to calculate dose rates are explained in the footnotes in Table 2.

3.3. Determining rates of horizontal and vertical crustal displacement

Geomorphic rates of vertical and horizontal crustal displacement are determined by dividing the offset of moraine ridges and fan surfaces by the TCN age determined for the respective surface. These rates are considered maximum rates in the sense that the TCN ages represent minimum estimates of the surfaces age of the analyzed geomorphic surface.

4. Detailed study areas

4.1. Los Zerpa and La Victoria moraines of Sierra Nevada

The well-preserved La Victoria and Los Zerpa laterofrontal moraines record the maximum extent of glaciation during the last glacial (Figs. 3 and 4). Schubert (1970, 1974, 1998) initially focused his extensive studies of the glacial characteristics and history of the Venezuelan Andes in the La Victoria, Los Zerpa and surrounding area. Samples for ^{10}Be TCN dating were collected from nine boulders along the crests of the two moraines. The sample locations and ages are marked on the aerial photograph in Fig. 4 and are listed in Table 1.

The Boconó fault offsets the Los Zerpa and La Victoria moraines (Fig. 4). Faulted moraines were first recognized here in the Andes by Cluff and Hansen (1969) and Schubert and Sifontes (1970). The mean ^{10}Be TCN age for the La Victoria moraines is 16.5 ± 1.6 ka (based on samples VEN19, VEN20, VEN21, and VEN23). We measured ^{10}Be from five boulders on the Los Zerpa moraine. Four of these samples have ages that form a relatively tight cluster (VEN25 –VEN28, 16.9 ± 1.3 ka). The VEN24 sample has an inferred age twice the others. Although the total number of samples is only four, we assume that VEN24 has inherited cosmogenic ^{10}Be, and does

not represent the same geologic event as samples VEN25-VEN28. We do not include VEN 24 in any further calculations.. The mean ages for the Los Zerpa and La Victoria moraines are statistically indistinguishable from each other; we conclude that both moraines represent the same glacial event. The mean age for both moraines is 16.7 ± 1.4 ka (n = 8). We ascribe geologic significance to the mean age of the two moraines because the individual boulder ages are reasonably well clustered, though note ongoing debate regarding interpretation of boulder ages continues (c.f. Heyman et al., 2011). The mean age is within 2σ of the maximum age of both moraines so the geologic interpretation of these ages is not dependent on whether we ascribe significance to the mean or the maximum.

4.2. La Culata moraines

The headwaters of the Río Mucujún and Río La González each display well-preserved glacial moraines, and those along the Río Mucujún are referred to herein as the moraines of La Culata (Fig. 5). The city of Mérida sits downstream from the moraines of La Culata at the confluence of Ríos Mucujún and Chama. Large laterofrontal moraines are present at La Culata above ~ 3200 m asl and locally delineate the maximum extent of glaciation during the last glacial (Figs. 5 and 6)**.** In addition, a smaller inset moraine is present ~ 1 km upstream from the older laterofrontal moraines (Fig. 6). Eight samples were collected from boulders along two separate older laterofrontal moraine crests; five samples were collected from the younger inset moraine (Fig. 6**)**. Samples taken from the crest of the older laterofrontal moraines yield an average ^{10}Be TCN age of 15.2 ± 0.9 ka (n = 8; samples VEN01-VEN06 and VEN 13-VEN 14). Samples VEN07 through VEN12 collected from a younger inset moraine yield a ^{10}Be TCN age of 14.1 ± 1.0 ka (n = 5). The younger age of the inset moraine, though not statistically significant, is consistent with the morphostratigraphy.

4.3. The glacial outwash and valley fill sediments of Río Chama

The city of Mérida is built upon a broad mesa constructed of rounded boulder gravel of fluvial origin that is locally referred to as the 'meseta' and sits at the confluence of the Ríos Mucujún and Chama (Figs. 5 and 7). The relatively broad width of the valley in which the meseta sits is attributed to its location in an extensional right-step in the Boconó fault trace (Schubert, 1980b; Giegengack, 1984). The incision of the meseta by the Río Chama, and accordingly the thickness of the meseta deposit, decreases from nearly 200 m at the northwestern limit of Mérida to less than ~ 125 m at the southwest limit of the Meseta, and to ~ 100 m southwestward to Ejido (Fig. 5 and 8).

Remnants of the valley-fill deposits that form the meseta are also preserved southwestward of Ejido (Figs. 5 and 9). Three samples for OSL dating were collected from the main glacial outwash deposits that comprise the meseta along the Río Chama southwest of the city of Mérida (Figs. 5 and 9). Inset terraces are present though we did not date those in this study. The deposits are composed primarily of well-rounded bouldery gravel with local lenses of medium and coarse sand (Fig. 9). Samples OSL 14-2 and 14-8 were collected from beds of fluvial sand about 5 m from the fill surfaces that are ~ 100 m above the Río Chama and date to 30.5 ± 2.5 ka and 29.5 ± 2.2 ka, respectively (Fig. 9). Sample OSL 14-8 was collected from a similar fluvial sand within the same deposit from which OSL 14-1 was sampled at 58 m below the surface and is older at about 36.5 ± 2.4 ka.

4.4. Geomorphic expression of rangefront thrust faults and progressive Quaternary landform development along the northwestern flank of the Venezuelan Andes: Tucanízón and Arapuey

The uplift of the Andes is recorded in faulted, uplifted, and terraced alluvial fans along the northwestern Andean rangefront, initially noted by Singer (1985) and Soulas (1985) near the town of Arapuey. A generalized map showing faulted Quaternary alluvial surfaces between Arapuey and Tucaní is shown in Fig. 10. Progressive Pleistocene offset is recorded by increasingly larger scarp heights registered across progressively older fan elements between Tucaní and Arapuey (Fig. 10). Holocene displacement along the length of the rangefront is recorded by lesser scarps on the order of several meters height preserved in the youngest fan surfaces along the rangefront (e.g., Figs. 10 and 11).

At Tucaní (Fig. 10), the higher and lower of two offset fan surfaces are truncated at the rangefront and are present at elevations of 120 and 40 m above the mouth of the Río Tucanízón, respectively (Fig. 12). Locally preserved are moderate and large boulders. We collected a set of six samples from these boulders for ^{10}Be TCN dating. The locations are shown in Fig. 10. The ^{10}Be TCN dates range from about 44 to 133 ka, and the average age is 86.7 ± 36.6. The spread of ^{10}Be dates on the Tucaní surface is quite large, likely from deep weathering because of the antiquity (> 100 ka) and the wetter and warmer climate at the low elevation of these surfaces.

5. Discussion

5.1. Moraine ages and glacial history

Sievers (1886) and Jahn (1925, 1931) first recorded evidence of glaciation in the Venezuelan Andes. The works of Schubert later described in greater detail the extent and location of moraines and associated deposits in the region, and these works remain a primary source of reference today (Schubert, 1970, 1974; Schubert and Valastro, 1974; Schubert, 1975, 1984; Schubert and Clapperton, 1990; Schubert, 1992, 1998). Schubert and Mahaney et al. (2000; 2007b), among others, recognized that the once-glaciated regions of the Andes exhibit two distinct moraine systems: one of which is generally limited to elevations of 2600 to 2800 m asl, and the other between 2900 and 3500 m asl. The lower moraine system is characterized by the occurrence of continuous vegetation and highly weathered till. In contrast, the higher moraine systems are less weathered, have sharp ridge crests, and rise in relief up to 150 m high (e.g., Figs. 4 and 6). Schubert further attributed the higher and better-preserved glacial deposits to the latest Pleistocene glaciation. The two sets are locally referred to as the early and late stades of the Mérida glaciation (Mahaney et al., 2007b). More recently Stansell et al. (2007b) interpreted the equilibrium snow-line altitude during the maximum extent of the glaciation during the last glacial to be ~ 3200 to 3500 m asl). The downward extent of the glacial landforms/deposits varies by as much as 500 m between humid and arid slopes of the region (Schubert, 1975).

Assessments of the age of the maximum extent of glaciation of the last glacial and interglacial cycles in the Venezuelan Andes are based upon radiocarbon ages extracted from sediments and soils in lacustrine and peat deposits accumulated following the retreat of glaciers in the high Andes northeast of Mérida (Figs. 2 and 3). These minimum ages constrain the time of moraine development. Schubert and Rinaldi (1987) extracted radiocarbon samples from the top and bottom of the 30-m exposure of glaciofluvial and lacustrine deposits near Mesa del Caballo (location shown in Fig. 3). The top of the exposure is at an elevation of ~ 3500 m asl. Using

301 radiocarbon dates of 16.5 ± 0.29 ka (19.0-20.3 cal ka @ 95% confidence) and 19.0 ± 0.82 ka BP
302 (20.6-25.0 cal ka @ 95.4% confidence) for the top and base of the 30-m exposed section,
303 respectively, Schubert and Rinaldi (1987) interpreted that glaciers filled (at least to a large
304 extent) their valleys at this time, and that the late Stade of the Mérida glaciation approximately
305 coincides with the global Last Glacial Maximum (LGM) at ~ 18-24 cal ka. (All radiocarbon
306 dates we calibrate are quoted to 95.4% probability using OxCal online calculator at
307 http://c14.arch.ox.ac.uk/embed.php?File=oxcal.html.) In the following discussion we assume the
308 timing of the global LGM is 19–23 cal ka at Chronozone level 1 or 18–24 cal ka at chronozone
309 level 2, according to the work of Mix *et al*. (2001). Whether mountain glaciers reach their
310 maximum extent coincident with continental ice sheets and global estimates of the LGM remains
311 a matter of discussion (see Gillespie and Molnar, 1995, and Thackray et al., 2008). For this
312 reason we also refer to the maximum extent of glaciers in the Venezuelan Andes as the local last
313 glacial maximum (LLGM).

314 Mahaney et al. (2001; 2004) collected an additional suite of samples for AMS radiocarbon from
315 the same section as Schubert and Rinaldi (1987) and provided a detailed sedimentological
316 analysis and description of the exposure. Like Schubert and Rinaldi, they observed that the
317 entire sequence was composed of glaciofluvial and glaciolacustrine sediments with interbedded
318 minor peats and paleosols. The dates they report for the section differ significantly with those
319 reported by Schubert and Rinaldi (1987). Mahaney et al. (2001; 2004) report ages at the top of
320 the section (~ 3 m below surface), at 26 to 29 m down section, and the basal 6 m of the section to
321 equal 12.95 ± 0.45 ka BP (14.1-16.9 cal ka), > 25.80 to 25.15 ± 0.40 ka BP (> 31.2 to 29.3-30.9
322 cal ka), and 47.84 ± 0.88 ka BP (out of range for calibration), respectively. We obtained a
323 similar radiocarbon age for a peat sample taken from the base of the section (>50,200 yr BP ;
324 CAMS #139847). The ponding and deposition of these sediments requires the presence of the
325 lateral moraines from not one but rather two adjacent glaciers, the moraines of La Mucachache
326 and Quebrada del Caballo (Fig. 3). The old age at the base of the section of ponded sediments
327 may indicate that the moraines are of an age greater than the global LGM. This uncertainty
328 motivated our efforts to date directly the age of rocks composing major glacial moraines of the
329 Venezuelan Andes.

330 A couple of kilometers to the east Stansell et al. (2005) more recently obtained radiocarbon ages
331 of sediment core sections from seven lakes and a couple of bogs to the northeast. These are
332 ponded behind and along the Mucubají moraines (Fig. 3) and to the north of Lago Mucabaji in
333 the Sierra Norte. Interpreting the onset of organic matter in the cores as the cessation of glacial
334 input, they suggested that significant retreat of the associated glaciers occurred by ~ 15.7 ka cal
335 BP in the Mucubají complex and ~ 14.2 ka cal BP at sites to the northwest and across of the
336 Boconó fault in the Sierra Norte. The later discussion of Mahaney et al. (2007a) and Stansell et
337 al. (2007a) elucidated uncertainities inherent in these studies. Regardless, the ages from the
338 lakes and bogs are best interpreted as limiting dates and proxies of time of the emplacement of
339 the major moraine complexes during the LLGM.

340 The La Victoria and Los Zerpa moraines are 5 km northeast of the Laguna Mucubají and the La
341 Mucuchache and El Caballo moraines in the Sierra Nevada (de Santo Domingo) (Fig. 3). The
342 surface exposure ages of rocks on the Los Zerpa and La Victoria moraines when taken together
343 place the age of the latest glacial maximum at 16.7 ± 1.4 ka in the Sierra Nevada (de Santo
344 Domingo). The moraines of La Culata within the Sierra Norte are about 25 km to the west and

situated across the Andean valley that follows the Boconó fault (Figs. 2, 3, and 6). The mean TCN ages for samples along the largest and most extensive La Culata lateral moraines are slightly younger (15.2 ± 0.9 ka) than the Los Zerpa and La Victoria moraines of the Sierra Nevada (16.7 ± 1.4 ka). The results suggest a component of asynchroneity in the occurrence of the LLGM between the Sierra Nevada and Sierra Norte. A yet later small readvance during the Late Glacial is suggested by the ages of samples VEN07 through 12 from a younger inset moraine that yield younger ages of 14.1 ± 1.0 ka.

The moraine ages measured here are consistent with Mahaney et al.'s (2001) observation that sediments ponded between the La Mucuchache and El Caballo moraines (Fig. 3) breached subsequent to the LLGM at about 12.95 ± 0.45 ka BP. Stansell et al. (2005) interprets significant retreat of moraines in the Sierra Norte occurred later (~ 14.2 ka cal BP) as compared to the Sierra Nevada (~ 15.7 ka cal BP). The age of the LLGM we find for the La Culata moraines of the Sierra Norte (15.2 ± 0.9 ka) is also less than the age of the LLGM we find for the Los Zerpa and La Victoria moraines of the Sierra Nevada (16.7 ± 1.4 ka), though not to a degree of statistical significance.

The role of the tropics in climate change and glacial cycles remains debated in large part because definitive glacial chronologies are largely lacking for most tropical regions. The ages we have determined for LLGM moraines in Venezuela may ultimately contribute to understanding the temporal relationship of glaciation in equatorial and higher latitudes, which in turn will lead to a greater appreciation of the factors that ultimately produce glacial cycles.

The ^{10}Be TCN ages we obtained for the LLGM moraines of Venezuela are broadly consistent with the Heinrich 1 event (H1) at ~ 16.8 ka (Hemming, 2004). The agreement is tempered by the uncertainty in calculating ^{10}Be TCN ages for high altitude tropical and equatorial regions is not known (Lowell et al., 2010) and the recognition that H1 might be younger (e.g., ~ 16.1 ka; Bard et al., 2000). Taking the available data at face value indicates that the LLGM of Venezuela occurred during HI. We also infer that the timing of glacier advances in the Venezuelan Andes is coeval to cold periods in the Northern Hemisphere as recorded in the Greenland ice core records and the North Atlantic marine record. The LLGM advance in the Venezuelan Andes is significantly younger than the global LGM at ~ 18-24 ka and is also later than glacial maxima in most other regions of the Andes (Smith et al., 2008; Thackray et al., 2008). Glaciers in Peru and Bolivia reached there greatest extent at ~ 34 ka and were retreating by ~ 21 ka (Smith et al., 2005). These latter differences may not be significant if, as suggested by Zech et al. (2008), glaciers in the northern, tropical parts of the central Andes were mainly temperature sensitive and advanced during temperature minimum, such as occurred during H1. Our ^{10}TCN data provide tentative support for the view that temperature changes in the Venezuelan Andes rather than precipitation changes were primary in driving glaciation in this region.

5.2. Boconó fault slip rate

Since the initial recognition of strike-slip faults in Venezuela (Rod, 1956a, b), numerous investigators have described aspects of the tectonic geomorphology along the Boconó fault in English (e.g., Cluff and Hansen, 1969; Giegengack and Grauch, 1972; Schubert, 1982; Schubert et al., 1992; Audemard et al., 2008) and Spanish publications (e.g., Schubert, 1980a; Giraldo, 1985; Singer, 1985; Soulas et al., 1986; Ferrer, 1991). The fault is marked by an abundance of aligned 1-5 km wide valleys, linear depressions, sidehill benches, saddles, trenches, sag ponds,

and scarps in young alluvium and moraines. Many of these are documented in Figs. 3 and 5. Prior estimates of the late Quaternary slip rate of the Boconó fault derived from measured offsets of selected Pleistocene moraines depicted in Figs. 3 and 4 and assumptions bearing on the age of the displaced moraines.

Schubert and Sifontes (1970) reported a first slip rate estimate of 6.6 mm a^{-1}. The estimate was based on the measurement of 66-m offsets across the La Victoria and Los Zerpa lateral moraine crests in the Mucubají region of the Sierra Nevada (Fig. 4) and the assumption that the moraines correlated to moraines in the Sabana de Bogotá, Colombia; these were then estimated to be formed at ~ 10 ka. Giegengack and Grauch (1972) reinterpreted the offsets to be 80-100 m and disputed the correlation to Colombian glaciers. Later summaries (e.g., Audemard et al., 1999; Audemard et al., 2008) reevaluated the same offsets to range from 60 to 100 m and assumed moraine ages of ~ 15 ka to interpret a fault slip rate of 5-9 mm a^{-1}. The basis of the assumed age for the Los Zerpa moraine is a radiocarbon date of 12.65 ± 0.13 ka BP from Salgado-Labouriau et al. (1977) for a sample taken from a section of peat exposed by a secondary normal fault that sits within the Laguna de Mucubají moraines (location noted in Fig. 3).

The Boconó fault consists of two subparallel strands in the Apartaderos area (Figs. 3 and 4); each displaces glacial moraines. Audemard et al. (1999) estimated the cumulative slip rate across the two strands at ~ 7-10 mm a^{-1}. The rate calculation was based on measurement of the moraine offsets and use of Salgado-Labouriau et al's (1977) radiocarbon date to interpret the age of the moraines to equal 15 ± 2 ka. Using dates of the two most recent earthquakes (of which the latter produced a 30-cm vertical displacement) coupled with 10°-20° slickenside orientations measured in a fault trench within a nearby gully where fault gouge crops out, Audemard (1997) also estimated that the fault slips at a rate of 5.2 ± 0.9 mm a^{-1} near La Grita (Fig. 1).

The ^{10}Be TCN ages determined for boulders on displaced moraine surfaces in our study provide an additional and direct constraint on the age and thus slip rate of the displaced Los Zerpa and La Victoria moraine crests (Figs. 3 and 4). The average ^{10}Be TCN age of boulders taken from these surfaces is 16.7 ± 1.4 ka (n = 8). Taking the maximum reported measures of fault offset of the Los Zerpa and La Victoria LLGM moraine crests summarized in Fig. 3 to equal 100 m, the observations point to a maximum slip rate of ~ 5.5 to 6.5 mm a^{-1}.

DeMets et al. (2010) reported geodetic constraints on the motion of the Caribbean-South America plate boundary. Relative plate motion between the South American and the Caribbean plates is about 18 mm a^{-1} (Fig. 1). A significant portion of this motion is taken up by right-lateral displacement along the Boconó fault. The recent work of Pérez et al. (2011) showed a well-defined though broad 80-km-wide zone of right-lateral shear centered along the Boconó fault. Modeling shows the shear signal may be explained by the equivalent of 12 ± 2 mm a^{-1} on a fault with locking depth between 14 ± 4 km. The geodetic rate is conspicuously greater than the rate we have estimated from the offset of the Los Zerpa and La Victoria moraines.

5.3. Thrust faulting along the Andean flanks

The presence of an abrupt range front (e.g. Figs. 1 and 2), fold structures expressed at the surface (e.g., Fig. 2), and subsurface reflection seismic data indicate the presence of active thrusting along the Andean rangefronts (Audemard and Audemard, 2002; Audemard, 2003). The presence of young scarps and progressively greater offset of older, faulted alluvial surfaces at Arapuey

(Singer, 1985; Soulas, 1985) and Tucaní (Fig. 10) attests to the repeated and recent uplift of the northwestern flank of the range. The range of ^{10}Be TCN dates for boulders on the Tucaní surface is broad with an average of 87 ± 37 ka (1σ). Dividing the 120-m scarp height of the Tucaní surface by the age yields a surface uplift rate of 1.7 ± 0.7 mm a^{-1}.

It is unclear whether the broad range of ages is due to inheritance or whether it reflects variations in rates of weathering and exposure of boulders on the surface. We favor the latter and the lower bound on the slip rate because the number of boulders on the Tucaní surface is few, the range of maximum boulder size varies markedly across the surface, and the rainfall and temperatures at the elevation of the surface are much greater than in the high once-glaciated Andes (Table 1). The Tucaní scarp is smooth and curved in map view (Fig. 10). A large active fan extends northwestward from the scarp and is the result of sedimentation associated with the Río Tucanízón (Fig 10). The fan-head elevation at the base of the Tucaní scarp approaches 90 m, but elevations are as low as 30 to 40 m elsewhere along strike at the base of the rangefront. Sea level rise may have been as much as 7 m during the last interglacial (Kopp et al., 2009). The proximity of the scarp to Lago Maracaibo and the presence of sedimentary fill at the base of the scarp allow consideration that the scarp may have once been modified by shore processes, in which case, the scarp height might be an overestimate of the actual offset. In contrast, the sediment fill at the base of the scarp by modern fan development represents a competing uncertainty that works to decrease the scarp height and the estimate of uplift rate.

Prior estimates of the rate of uplift of the Venezuelan Andes include (i) Kohn et al.'s (1984) use of cooling ages from apatite fission tract analysis to estimate the rate at 0.8 mm a^{-1} over the last 800,000 years; (ii) Shagam et al.'s (1984) simultaneous interpretation that the Andes has uplifted 4000 m over the same time period suggesting a greater uplift rate of ~ 5 mm a^{-1}; and (iii) Audemard's (2003) synthesis of the geologic observations of others to interpret 13-15 km of uplift has occurred in the last 3-5 Ma leading to an uplift rate estimate of 2.6-5.0 mm a^{-1}. Bermúdez et al. (2010) recently have used apatite fission track thermochronology to place the onset of central Andean uplift at > 8 Ma, perhaps suggesting that the last of the prior rate estimates is overestimated. The broad range of these uplift rate values and those calculated here for the late Pleistocene preclude assessment of whether or not uplift rates have been steady through time.

The geodetic measurements recently reported by Pérez et al. (2011) also show a component of convergence in the contemporary strain signal across the Andes. Across the section of Andes encompassing our study, the amount of convergence is on the order of 2 mm a^{-1} and likely accommodated by reverse faults possibly within and along the flanks of the Andes. The uplift rate we have determined from the offset Tucaní fan is 1.7 ± 0.7 mm a^{-1}. Presuming that the uplift is occurring on a fault of dip between 30° and 45°, the uplift rate is equivalent to a horizontal shortening rate of 2.5 ± 1.5 mm a^{-1}. Our sense is that the oldest dates on the Tucaní surface more closely reflect the actual age of the surface and, for that reason, we are favor the lower end of the age range. If so, the geologic rate is generally consistent with that indicated by geodesy. A more extensive sampling of rocks and ages on this and additional fan surfaces as well as further geodetic observation will be required to reduce the uncertainty of measurements to yield more resolution to such comparisons.

5.4. Valley-fill deposits of Mérida and the Río Chama

The valley-fill deposits of the meseta surface at Mérida and along the Río Chama provide data on the nature of sediment transfer from the high mountains to the Andean foreland. The thickness of the meseta deposit (approaching 200 m) at the confluence of the Ríos Chama and Mucujun, the continuation of the terrace surface upstream along the Río Mucujun, and the decreasing thickness of the deposit downstream indicate that outwash of the moraines of La Culata were primary in contributing to the development of the meseta. In this regard, the meseta is constructed of glacial outwash deposits; and the large scarps associated with the incision of the meseta are not a reflection of tectonic uplift but rather simply a change in stream energy, competency, and capacity resulting from a change in climate. A smaller analog to the meseta occurs at San Rafael where the Quebrada de Fria has transported sediment to the Rio Chama , creating a terrace ~ 100 m high that decreases southwestward in elevation and thickness along the Rio Chama and forms the surface on which San Rafael is located (Fig. 5).

Samples extracted from near the surface of valley-fill deposits that form the meseta (Figs. 5 and 7) and terraces southwestward along the Rio Chama to Lagunillas (Figs. 5, 7, and 9) have OSL dates of 30.5 ± 2.5 ka and 29.5 ± 2.2 ka . When coupled with the 36.5 ± 2.4 ka OSL age of the sample 58 m below the surface, the OSL ages allow the suggestion that the majority and final aggradation of valley fill deposits on which the Meseta is formed occurred quite rapidly over a period of about 5 to 6 ka and that the surface was initially incised and abandoned ~30 ka ago. The aggradation, eventual incision, and thus abandonment of the deposits probably occurred some 15 ka prior to the LLGM and retreat of the moraines of La Culata (Figs 5 and 6) and the Sierra Nevada (Figs 3 and 4).

5.5 Active deformation

The studies of Schubert (1982, 1992) document the tectonic geomorphology associated with late Pleistocene slip along the Boconó fault. Paleoseismic studies since that time (e.g., Audemard, 2005) have further demonstrated that the Boconó fault has been active throughout the Quaternary and that sections of the fault produce large earthquakes on the order of every 200-300 years. The Boconó fault slip rate estimate of ~ 5.5 to 6.5 mm a^{-1} determined here is the first to arise from direct dating of the offset glacial moraines. The rate is significantly less than the 12 ± 2 mm/y being recorded across the Andes with geodesy (Pérez et al., 2011). The difference may reflect a systematic error in the ^{10}Be TCN ages. For the following reason we do not favor this explanation. To arrive at a geologic slip rate equal to that predicted by geodesy requires the age of the moraines to be half what we have estimated from TCN analysis or, likewise, the LLGM to be as recent as 8 ka. The close agreement (within uncertainties) between moraine ages across our study area provides some level of confidence that the TCN ages are reliable and indeed reflect closely the age of the moraine surfaces. More likely, and as pointed out in Pérez et al. (2011), the Boconó fault is only accommodating a portion (~1/2) of the displacement within the broad ~ 80-km-wide zone of deformation currently defined by geodesy. Determining the faults and the respective slip rates of those faults on which the missing shear component is distributed fell beyond the scope allowed by our project. Nearby mapped faults likely accommodating some portion of the slip budget include elements of the subparallel Valera and Tuname fault systems, each with reported slip rates up to 0.5 to 1 mm/y (Audemard et al., 2000). Right-lateral shear may also be taken up by an as yet unrecognized lateral component of slip on the Andean rangebounding thrusts. In sum, the Boconó fault is apparently accounting for only about one-half of the geodetic slip budget and, hence, seismic hazard across the Andes in the vicinity of our study.

Likewise, prior efforts have shown the flanks of the Andes to exhibit clear evidence of continued thrusting and associated uplift during the Quaternary (Singer, 1985; Soulas, 1985; Audemard and Audemard, 2002; Audemard, 2003). Our observations and documentation of youthful scarps and progressive offsets in Quaternary deposits along both flanks of the Andes compliment these observations. The Andean flank faults are commonly cited as 'blind,' yet the observations presented by Singer (1985) and Soulas (1985) and here suggest that the presence of fault-truncated fans and terraces and youthful scarps in young alluvium are common along both flanks (Figs 10, 11, and 13). The situation is similar to that observed for the main bounding thrust fault of the Himalaya where folding is common, and the apparent absence of young scarps led earlier workers to interpret it to be 'blind' (e.g., Stein and Yeats, 1989), while yet later studies confirmed the fault to commonly produce scarps at the surface, and trench exposures have documented surface displacements of 10 to 15 m and greater (Kumar et al., 2006, 2010). We surmise the next large earthquake will produce surface rupture and thus surface rupture hazard to lifelines along the full length of the rupture.

The uplift rate of 1.7 ± 0.7 mm a^{-1} we estimate at Tucaní allows an estimate of the slip rate of the thrust fault bounding the northwest flank of the Andes. Allowing the thrust dips as low as 30° and as steep as 45°, a fault slip rate of 3.1 ± 1.7 mm a^{-1} is required to produce the 1.7 ± 0.7 mm a^{-1} uplift rate. The uncertainty in the slip rate is quite broad but, nonetheless when coupled with the presence of youthful scarps and evidence of continued offset on both sides of the ranges, points to a significant seismic hazard on both flanks of the Andes that has perhaps not gained a level of attention like that for the Boconó fault. Given the uplift rate estimate of 1.7 ± 0.7 mm a^{-1}, it would take about one to three thousand years to accumulate the slip represented in the smallest of youthful scarps observed (~ 3 m). The value can be viewed as a maximum bound on the return time of earthquakes along sections of the rangefront because these smaller scarps may be the result of more than one displacement.

6. Conclusions

The dating of landforms presented here is intended to contribute to the discussion and understanding of issues and topics that range from processes of landscape development to the history of glaciation, neotectonics, and seismic hazard of Venezuela. The surface exposure ages on moraines within the Sierra Nevada and Sierra Norte place the age of the LLGM at 15.9 ±1.4 ka (n = 16, average of La Culata, Los Zerpa, and La Victoria moraine boulders), with evidence for a small readvance at 14.1 ± 1.0 ka. The estimate of the age of the LLGM is in accord with younger and limiting ages previously reported from radiocarbon ages of sediments deposited subsequent to the LLGM (Stansell et al., 2005; Mahaney et al., 2007b). At a regional scale, the surface exposure ages of the dated moraines of La Culata within the Sierra Norte (15.2 ± 0.9 ka, n = 8) have slightly younger ages than those found on the Los Zerpa and La Victoria moraines (16.7 ± 1.4 ka, n = 8) within the Sierra Nevada and suggest some regional topographic control and asynchroneity in the LLGM across the Venezuelan Andes. The difference in the Venezuela LLGM measurements with those reported in the Andes of Peru and Bolivia to the south suggests even greater regional asynchroneity in the LLGM (Smith et al., 2005, 2008).

The dating of glacial outwash and valley-fill sediments that currently form terraces > 100 m height along the Rio Chama within the central Andean valley, and on which the major city of Merida is built (the 'meseta'), provides an initial glimpse at processes of sediment transfer and

how it here relates to the timing of the LLGM. At and downstream from Merida, the valley fill deposits appear to have been largely deposited over a period on the order of 5 to 6 ka and to be initially incised and abandoned at ~ 30 ka. The observations also suggest that valley-fill sediments are episodically stored and rapidly deposited and transported through the Venezuelan Andes, probably on Milankovitch timescales, influenced by glaciation. The fill deposits appear to have occurred significantly earlier than the LLGM and suggest complex links between climate, glaciation, and sediment transfer that will only be answered with further examples and research.

Measured fault displacement of the Los Zerpa and the La Victoria moraines divided by the surface exposure ages of the respective moraine surfaces places the slip rate of the Boconó fault at less than ~ 5.5 to 6.5 mm a^{-1}. This measure of the slip rate derived from direct dating of the offset moraine surfaces is within the range of prior estimates where ages of the displaced moraines were assumed with correlation to the timing of glaciation elsewhere or limiting ages derived from radiocarbon ages of sediments ponded behind moraines subsequent to the LLGM. The slip rate is markedly lower than the 12 ± 2 mm a^{-1} that has recently been documented across the ~ 80-km width of the Andes from geodesy (Pérez et al., 2011). The majority, if not all, of the difference is likely due to yet unaccounted for displacement on other active faults within and along the flanks of the Andes

The presence of youthful scarps in young sediments and yet higher, older, faulted alluvial surfaces on both flanks of the Andes records continuous late Quaternary displacement along the thrust faults that bound the Andes. Geophysical studies show that structural accommodation of convergence across the Andes is complex and accommodated by 'blind' thrusts that do not reach to the surface (DeToni and Kellogg, 1993; Audemard, 2005). Nonetheless, the presence of an abrupt rangefront, the truncations of fluvial terraces at the rangefront (Figs. 10 & 13), and the presence of sharp youthful fault scarps along the rangefront indicate the main bounding thrusts commonly emerge to the surface (e.g. Figs. 11 and 13), a situation akin to that observed along the main Himalayan thrust of India (Wesnousky et al., 1999; Kumar et al., 2008; Kumar et al., 2010). The ~ 120-m scarp height of the Tucaní fan surface and the surface exposure ages of boulders preserved on the surface allow an initial approximation of the uplift rate at 1.7 ± 0.7 mm a^{-1} and equivalently, if the fault dips at 30°-45°, horizontal convergence and fault slip rates of 2.5 ± 1.5 mm a^{-1} and 3.1± 1.7 mm a^{-1}, respectively.

Acknowledgements

The mapping was largely accomplished while one of us (SGW) was hosted by the Laboratorio de Geofísica of the Universidad de los Andes in Mérida while supported on a Fulbright Fellowship in 2005. A special thanks goes to José Choy and Stephanie Klaric, then Coordinators of LG-ULA, and Nelson Viloria, Dean of the Facultad de Ciencias, for their support of this research. SGW benefited from partial suupport of the research by the UNR Foundation. Sampling was accomplished by all of us in July 2008. Inability to gain further support precluded initiation of more detailed mapping and collection of more samples, and we thus chose to present here the data we did collect. The authors gratefully acknowledge the efficiency and editing of Richard Marston and the comments of 3 anonymous reviewers. Last but not least, we thank Daniel for keeping the Fiesta running and the hospitality of the Guada family while in Venezuela. Center for Neotectonics Contribution 64. The NSF for not funding this research.

References

Adamiec, G., Aitken, M., 1998. Dose-rate conversion factors: update. Ancient TL 16, 37-50.

Aitken, M.J., 1998. An Introduction to Optical Dating. Oxford University Press, Oxford, U.K., 280. pp.

Amante, C., Eakins, B.W., 2009. ETOPO1 1 Arc-minute global relief model: procedures, data sources and analysis. NOAA Technical Memorandum NGDC-24, pp. 19

Audemard, F.A., 1997. Holocene and historical earthquakes on the Bocono fault system, southern Venezuelan Andes: trench confirmation. Journal of Geodynamics 24, 155-167.

Audemard, F.A., Pantosti, D., Machette, M., Costa, C., Okumura, K., Cowan, H., Diederix, H., Ferrer, C., Acosta, L., Alvarado, A., Arzola, A., Drake, L., Gardini, C., Gomez, I.C., Laffaille, J., Perez, A.M., Rengifo, M., Saadi, A., Vergara, H., Paleoseisomology, S.A.F.W., 1999. Trench investigation along the Merida section of the Boconó fault (central Venezuelan Andes), Venezuela. Tectonophysics 308, 1-21.

Audemard, F.A., Machette, M.N., Cox, J.W., Dart, R.L., Haller, K.M., 2000. Map and database of Quaternary faults in Venezuela and its offshore regions. U. S. Geological Survey Open File Report 00-018, Denver, CO, p. 82

Audemard, F.A., 2003. Geomorphic and geologic evidence of ongoing uplift and deformation in the Merida Andes, Venezuela. Quaternary International 101, 43-65.

Audemard, F.A., 2005. Paleoseismology in Venezuela: objectives, methods, applications, limitations and perspectives. Tectonophysics 408, 29-61.

Audemard, F.A., Ollarves, R., Bechtold, M., Diaz, G., Beck, C., Carrillo, E., Pantosti, D., Diederix, H., 2008. Trench investigation on the main strand of the Boconó fault in its central section, at Mesa del Caballo, Mérida Andes, Venezuela. Tectonophysics 459, 38-53.

Audemard, F.E., Audemard, F.A., 2002. Structure of the Mérida Andes, Venezuela: relations with the South America-Caribbean geodynamic interaction. Tectonophysics 345, 299-327.

Balco, G., Stone, J.O., Lifton, N.A., Dunai, T.J., 2008. A complete and easily accessible means of calculating surface exposure ages or erosion rates from 10Be and 26Al measurements. Quaternary Geochronology 8, 174-195.

Bard, E., Rostek, F., Turon, J.L., Gendreau, S., 2000. Hydrological impact of Heinrich events in the subtropical northeast Atlantic. Science 289, 1321-1324.

Bermúdez, M.A., Kohn, B.P., van der Beek, M., Bernet, P.B., O'Sullivan, P.A., Shagam, R., 2010. Spatial and temporal patterns of exhumation across the Venezuelan Andes: Implications for Cenozoic Caribbean geodynamics. Tectonics 29(TC50009), 21, doi:10.1029/2009C002635.

Cluff, L., Hansen, W., 1969. Seismicity and seismic geology of Northwestern Venezuela. Unpublished report for Shell de Venezuela. Woodward-Clyde and Associates, San Francisco, CA, pp. 78.

DeMets, C., Gordon, R.G., Argus, D.F., 2010. Geologically current plate motions. Geophys. J. Int. 181, 1-80.

DeToni, B., Kellogg, J., 1993. Seismic evidence for blind thrusting of the northwestern flank of the Venezuelan Andes. Tectonics 12, 1393-1409.

Ferrer, C., 1991. Caracterısticas geomorfológicas y Neotectónicas de unsegmento de la falla de Boconó entre la ciudad de Mérida y la Laguna de Mucubají. Guía de la excursion, Escuela Latinoamericana de Geofísica Volume 25.
Giegengack, R., Grauch, R.I., 1972. Bocono fault, Venezuelan Andes. Science 175, 558-561.
Giegengack, R., 1984. Late Cenozoic tectonic environments of the central Venezuelan Andes. Geological Society of America Memoirs 162, 343-364.
Gillespie, A., Molnar, P., 1995. Asynchronous maximum advances of mountain and continental glaciers. Reviews of Geophysics 33, 311-364.
Giraldo, C., 1985. Neotectónica y sismotectónica de la region de El Tocuy San Felipe (Venezuela centro-occidental). VI Congreso Geológico, Venezolano 4, 351-357.
Gosse, J.C., Phillips, F.M., 2001. Terrestrial in situ cosmogenic nuclides: theory and application. Quaternary Science Reviews 20, 1475-1560.
Heisinger, B., Lal, D., Jull, A.J.T., Kubik, P., Ivy-Ochs, S., Knie, K., Nolte, E., 2002a. Production of selected cosmogenic radionuclides by muons: 2. Capture of negative muons. . Earth and Planetary Science Letters 200, 357-369.
Heisinger, B., Lal, D., Jull, A.J.T., Kubik, P., Ivy-Ochs, S., Neumaier, S., Knie, K., Lazarev, V., Nolte, E., 2002b. Production of selected cosmogenic radionuclides by muons 1. Fast muons. Earth and Planetary Science Letters 200, 345-355.
Hemming, S.R., 2004. Heinrich events: massive late Pleistocene detritus layers of the north Atlantic and their global climate imprint. Reviews of Geophysics 42, RG1005: DOI: 10.1029/2003RG000128.
Heyman, J., Stroeven, A., Harbor, J., Caffee, M.W., 2011. Too young or too old: evaluating cosmogenic exposure dating based on an analysis of compiled boulder exposure ages. Earth and Planetary Science Letters 302, 71-80.
Jahn, A., 1912. Orografía de la cordillera Venezolana de los Andes. Revista Técnica del Ministerio de Obras Publicas de Venezuela 2, 451-468.
Jahn, A., 1925. Observaciones glaciológicas en los Andes venezolanos. Cultura Venezolana 18, 265-280.
Jahn, A., 1931. El deshielo de la Sierra Nevada de Méreida y sus causas. Cultura Venezolana 110, 5-15.
Kohn, B., Shagam, R., Banks, P., Burkley, L., Kohn, B., Shagam, R., Banks, P., Burkley, L., 1984. Mesozoic-Pleistocene fission track ages on rocks of the Venezuelan Andes and their tectonic implications. Geological Society of America Memoir 162, 365-384.
Kopp, R.E., Simons, F.J., Mitrovica, J.X., Maloof, A.C., Oppenheimer, M., 2009. Probabilistic assessment of sea level during the last interglacial stage. Nature 462, 863-867.
Kumar, S., Wesnousky, S.G., Rockwell, T.K., Briggs, R.W., Thakur, V.C., Jayangondaperumal, R., 2006. Paleoseismic evidence of great surface-rupture earthquakes along the Indian Himalaya. Journal of Geophysical Research 111, B03304, doi:10.1029/2004JB003309.
Kumar, S., Wesnousky, S.G., Jayangondaperumal, R., Nakata, T., Kumahara, Y., Singh, V., 2008. Paleoseismological evidence of surface faulting along the northeastern Himalayan front, India: timing, size, and extent of great earthquakes. Himalayan Geology 29, 46-46.
Kumar, S., Wesnousky, S.G., Jayangondaperumal, R., Nakata, T., Kumahara, Y., Singh, V., 2010. Paleoseismological evidence of surface faulting along the northeastern Himalayan front, India; timing, size, and spatial extent of great earthquakes. Journal of Geophysical Research 115, doi:10.1029/2009JB006789.

693 Lal, D., 1991. Cosmic ray labeling of erosion surfaces: in situ nuclide production rates and
694 erosion models. Earth and Planetary Science Letters 104, 429–439.
695 León, G.A.D., 2001. Los picos más altos del estado Mérida-Venezuela (The highest peaks in
696 Mérida State-Venezuela). Rev. Geog. Venez. 42, 73-97.
697 Lowell, T.V., Kelly, M.A., Applegate, P.J., Smith, C.A., Phillips, F.M., Hudson, A.M., 2010.
698 Timing of expansions of the Quelccaya Ice Cap, Peru, and implications for cosmogenic
699 nuclide production rate calibration. American Geophysical Union, Washington D. C.,
700 Abstract EP32A-05.
701 Mahaney, W.C., Milner, M.W., Voros, J., Kalm, V., Hutt, G., Bezada, M., Hancock, R.G.V.,
702 Aufreiter, S., 2000. Stratotype for the Merida Glaciation at Pueblo Llano in the northern
703 Venezuelan Andes. Journal of South American Earth Sciences 13, 761-774.
704 Mahaney, W.C., Russell, S.E., Milner, M.W., Kalm, V., Bezada, M., Hancock, R.G.V., Beukens,
705 R.P., 2001. Paleopedology of middle Wisconsin-Weichselian paleosols in the Merida
706 Andes, Venezuela. Geoderma 104, 215-237.
707 Mahaney, W.C., Dirszowsky, R.W., Milner, M.W., Menzies, J., Stewart, A., Kalm, V., Bezada,
708 M., 2004. Quartz microtextures and microstructures owing to deformation of
709 glaciolacustrine sediments in the northern Venezuelan Andes. Journal of Quaternary
710 Science 19, 23-33.
711 Mahaney, W.C., Dirszowsky, R.W., Kalm, V., 2007a. Comment: Late Quaternary deglacial
712 history of the Mérida Andes, Venezuela. Journal of Quaternary Science 22, 817-821.
713 Mahaney, W.C., Dirszowsky, R.W., Milner, M.W., Harmsen, R., Finkelstein, S.A., Kalm, V.,
714 Bezada, M., Hancock, R.G.V., 2007b. Soil stratigraphy and plant-soil interactions on a
715 Late Glacial-Holocene fluvial terrace sequence, Sierra Nevada National Park, northern
716 Venezuelan Andes. Journal of South American Earth Sciences 23, 46-60.
717 Mejdahl, M., 1979. Thermoluminescence Dating: Beta Dose attenuation in quartz grains.
718 Archaeometry 21, 61-71.
719 Meteorological.Office, 2011. Venezuela: past weather and climate.
720 http://www.metoffice.gov.uk/weather/samerica/venezuela_past.html.
721 Mix, A.C., Bard, E., Schneider, R., 2001. Environmental processes of the ice age: land, ocean,
722 glaciers (EPILOG). Quaternary Science Reviews 20, 627-657.
723 Murray, A.S., Wintle, A.G., 2000. Luminescence dating of quartz using an improved single-
724 aliquot regenerative-dose protocol. Radiation Measurements 32, 57-73.
725 Nishiizumi, K., Imamura, M., Caffee, M.W., Southon, J.R., Finkel, R.C., McAninch, J., 2007.
726 Absolute calibration of 10Be AMS standards. Nuclear Instruments & Methods Physics
727 Research–Beam Interactions with Materials and Atoms 258B, 403-413.
728 Owen, L.A., Frankel, K.L., Knott, J.R., Reynhout, S., Finkel, R.C., Dolan, J.F., Lee, J., 2011a.
729 Beryllium-10 terrestrial cosmogenic nuclide surface exposure dating of Quaternary
730 landforms in Death Valley. Geomorphology 125, 541-557.
731 Owen, L.A., Frankel, K.L., Reynhout, S., Dolan, J.F., Finkel, R.C., 2011b. Dating Quaternary
732 surfaces in Death Valley using 10Be cosmogenic nuclides: problems and solutions.
733 Quaternary Science Reviews in press.
734 Pérez, O., Hoyer, M., Hernandez, N., Rodbell, D.T., Marques, V., Sue, N., Velandia, J.R.,
735 Delros, D., 2005. Alturas del Pico Bolivar y otras cimas andinas venezlanas a partir de
736 observaciones GPS. Interciencia 4, 213-216.
737 Pérez, O.J., Aggarwal, Y.P., 1981. Present-day tectonics of the southeastern Caribbean and
738 northeastern Venezuela. Journal of Geophysical Research 86, 10791-10804.

739 Pérez, O.J., Sanz, C., Lagos, G., 1997. Microseismicity, tectonics and seismic potential in
740 southern Caribbean and northern Venezuela. Journal of Seismology 1, 15-28.
741 Pérez, O.J., 1998. Seismological report on the Mw = 6.8 strong shock of 9 July 1997 in Cariaco,
742 northeastern Venezuela. Bulletin of the Seismological Society of America 88, 874-879.
743 Pérez, O.J., Bilham, R., Sequera, M., Molina, L., Gavotti, P., Codallo, H., Moncayo, C.,
744 Rodriguez, C., Velandia, R., Guzman, M., Molnar, P., 2011. Gps Derived Velocity Field
745 in Western Venezuela: Dextral Shear Component Associated to the Bocono Fault and
746 Convergent Component Normal to the Andes. Interciencia 36, 39-44.
747 Pigati, J.S., Lifton, N.A., 2004. Geomagnetic effects on time-integrated cosmogenic nuclide
748 production with emphasis on in situ 14C and 10Be. Earth and Planetary Science Letters
749 226, 193-205.
750 Pindell, R.L., Higgs, R., Dewey, J.F., 1998. Cenozoic palinspastic reconstruction,
751 paleogeographic evolution and hydrocrbon setting of the northern margin of South
752 America. Geographic evolution and non-glacial eustasy, Northren South America. SEPM
753 Special Publication 58, 45-85.
754 Prescott, J.R., Hutton, J.T., 1988. Cosmic ray and gamma ray dosimetry for TL and ESR.
755 Nuclear Tracks and Radiation Measurements. Nuclear Tracks and Radiation
756 Measurements 14, 223-230.
757 Putkonen, J., Swanson, T., 2003. Accuracy of cosmogenic ages for moraines. Quaternary
758 Research 59, 255-261.
759 Rod, E., 1956a. Strike-slip faults of northern Venezuela. Bulletin of American Association of
760 Petroleum Geologists 40, 457-476.
761 Rod, E., 1956b. Earthquakes of Venezuela related to strike slip faults? Bulletin of American
762 Association of Petroleum Geologists 40, 2509-2512.
763 Salgado-Labouriau, M.L., Schubert, C., Valastro, S., 1977. Paleoecologic analysis of a Late
764 Quaternary terrace from Mucubaji, Venezuelan Andes. Journal of Biogeography 4, 313-
765 325.
766 Schubert, C., 1970. Glaciation of the Sierra de Santo Domingo, Venezuelan Andes. Quaternaria
767 13, 225-246.
768 Schubert, C., Sifontes, R.S., 1970. Boconó-Fault, Venezuelan Andes - Evidence of Postglacial
769 Movement. Science 170, 66-69.
770 Schubert, C., 1974. Late Pleistocene Mérida glaciation Venezuelan Andes. Boreas 3, 147-152.
771 Schubert, C., Valastro, S., 1974. Late Pleistocene glaciation of Paramo de La Culata, north-
772 central Venezuelan Andes. Sonderdruck aus der Geologischen Rundschau 63, 517-537.
773 Schubert, C., 1975. Glaciation and periglacial morphology in the Northwestern Venezuelan
774 Andes. Eiszeitalter Gegenwart 26, 196-211.
775 Schubert, C., 1980a. Morfología Neotectónica de una falla rumbo-deslizante e informe
776 preliminar sobre la falla de Boconó, Andes merideños. Acta Cientifica Venezolana 31,
777 98-111.
778 Schubert, C., 1980b. Late-Cenozoic Pull-Apart Basins, Boconó Fault Zone, Venezuelan Andes.
779 Journal of Structural Geology 2, 463-468.
780 Schubert, C., 1982. Neotectonics of Boconó Fault, Western Venezuela. Tectonophysics 85, 205-
781 220.
782 Schubert, C., 1984. The Pleistocene and recent extent of the glaciers of the Sierra Nevada de
783 Mérida, Venezuela. Erdwiss. Forsch. 18, 269-278.

784 Schubert, C., Rinaldi, M., 1987. Nuevos Datos Sobre La Cronología del Estadio Tardio de la
785 Glaciaacion Mérida, Andes, Venezolanos. Acta Cientifica Venezolana 38, 135-136.
786 Schubert, C., Clapperton, C.M., 1990. Quaternary Glaciations in the Northern Andes (Venezuela,
787 Colombia and Ecuador). Quaternary Science Reviews 9, 123-135.
788 Schubert, C., 1992. The glaciers of the Sierra Nevada de Mérida (Venezuelan Andes).
789 Eiszeitalter Gegenwart 26, 196-211.
790 Schubert, C., Estevez, R., Henneberg, H., Buckman, R.C., Hancock, P.L., 1992. The Boconó
791 Fault, western Venezuela. Annales Tectonicae 6, 238-260.
792 Schubert, C., 1998. Glaciers of Venezuela. U.S. Geological Survey Professional Paper (
793 http://pubs.usgs.gov/prof/p1386i/venezuela/text.html) 1386-I, , 1-10.
794 Seong, Y.B., Owen, L.A., Bishop, M.P., Bush, A., Clendon, P., Copland, L., Finkel, R., Kamp,
795 U., Shroder, J.F., 2007. Quaternary glacial history of the central Karakoram. Quaternary
796 Science Reviews 26, 3384-3405.
797 Shagam, R., Kohn, B., Banks, P., Dasch, L., Vargas, R., Rodriquez, G., Pimentel, N., 1984.
798 Tectonic implications of Cretaceous-Pliocene fission track ages from rocks of he cicum-
799 Maracaibo Basin region of wesern Venezuela and eastern Colombia. Geological Society
800 of America Memoir 162, 385-412.
801 Sievers, W., 1886. Über Schneeverhältnisse in der Cordillere Venezuelas [On snow conditions in
802 the Venezuelan Cordillera]. Jahresbericht der Geographischen Gesellschaft in München,
803 1885, p. 54-57.
804 Singer, A., 1985. Evidencias geomorfologicas de fallamiento inverso en el Cuaternario del
805 piedemonte occidental de Los Andes Venozolanos. Congreso Geológico Venezolano,
806 Caracas 4, 2680-2689.
807 Smith, J.A., Seltzer, G.O., Farber, D.L., Rodbell, D.T., Finkel, R.C., 2005. Early local last glacial
808 maximum in the tropical Andes. Science 308, 678-681.
809 Smith, J.A., Mark, B.G., Rodbell, D.T., 2008. The timing and magnitude of mountain glaciation
810 in the tropical Andes. Journal of Quaternary Science 23, 609-634.
811 Soulas, J.P., 1985. Neotectónica del flanco occidental de los Andes de Venezuela entre 70°30' y
812 71°00'W (Fallas de Boconó, Valera, Piñango y del Piedemonte). Congreso Geológico
813 Venezolano, Caracas 4, 2690-2711.
814 Soulas, J.P., Rojas, C., Schubert, C., 1986. Neotectónica de las fallas de Bocono, Valera,
815 Tuname y Mene Grande. Journal 10(Issue): 6961-6999.
816 Staiger, J., Gosse, J., Toracinta, R., Oglesby, B., Fastook, J., Johnson, J.V., 2007. Atmospheric
817 scaling of cosmogenic nuclide production: climate effect. Journal of Geophysical
818 Research 112, B02205, doi:10.1029/2005JB003811.
819 Stansell, N.D., Abbott, M.B., Polissar, P.J., Wolfe, A.P., Bezada, M., Rull, V., 2005. Late
820 Quaternary deglacial history of the Merida Andes, Venezuela. Journal of Quaternary
821 Science 20, 801-812.
822 Stansell, N.D., Abbott, M.B., Polissar, P.J., Wolfe, A.P., Bezada, M., Rull, V., 2007a. Reply:
823 Late Quaternary deglacial history of the Mérida Andes, Venezuela: response to comment.
824 Journal of Quaternary Science 22, 823-825.
825 Stansell, N.D., Polissar, P.J., Abbott, M.B., 2007b. Last glacial maximum equilibrium-line
826 altitude and paleo-temperature reconstructions for the Cordillera de Merida, Venezuelan
827 Andes. Quaternary Research 67, 115-127.
828 Stein, R.S., Yeats, R.S., 1989. Hidden Earthquakes. Scientific American 260, 48-67.

829 Stone, J.O., 2000. Air pressure and cosmogenic isotope production. Journal of Geophysical
830 Research 105, 23753–23759.
831 Sykes, L.R., McCann, W.R., Kafka, A.L., 1982. Motion of Caribbean plate during last 7 million
832 years and implications for earlier Cenozoic movements. Journal of Geophysical Research
833 87, 10,656-10,676.
834 Thackray, G.D., Owen, L.A., Yi, C.L., 2008. Timing and nature of late Quaternary mountain
835 glaciation. Journal of Quaternary Science 23, 503-508.
836 Wesnousky, S.G., Kumar, S., Mohindra, R., Thakur, V.C., 1999. Holocene slip rate of the
837 Himalayan Frontal Thrust of India, Observations near Dehra Dun. Tectonics 18, 967-
838 976.
839 Zech, R., May, J.H., Kull, C., Ilgner, J., Kubik, P.W., Veit, H., 2008. Timing of the late
840 Quaternary glaciation in the Andes from ~15° to 40°S. Journal of Quaternary Science 23,
841 635-647.
842
843
844

844
845 **Figure Captions**
846

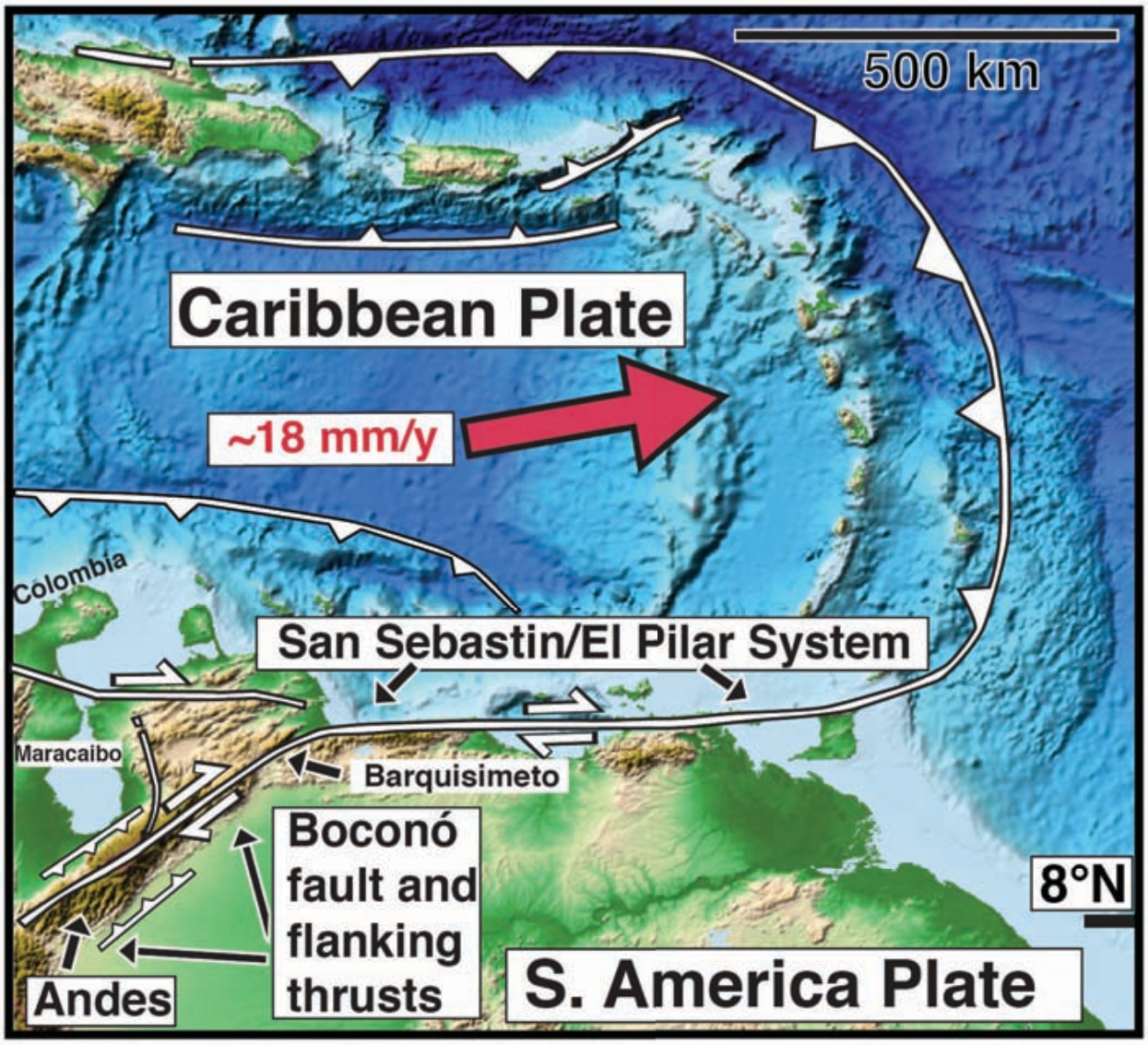

847
848 Fig. 1. Location map of Venezuelan Andes and Boconó fault system. Base map from Amante
849 and Eakens (2009). Major faults, plate boundary, and plate motion of Caribbean Plate with
850 respect to South American plate from DeMets et al. (2010). Triangles on hanging wall of thrust
851 faults. Half-sided arrows show direction of strike-slip.

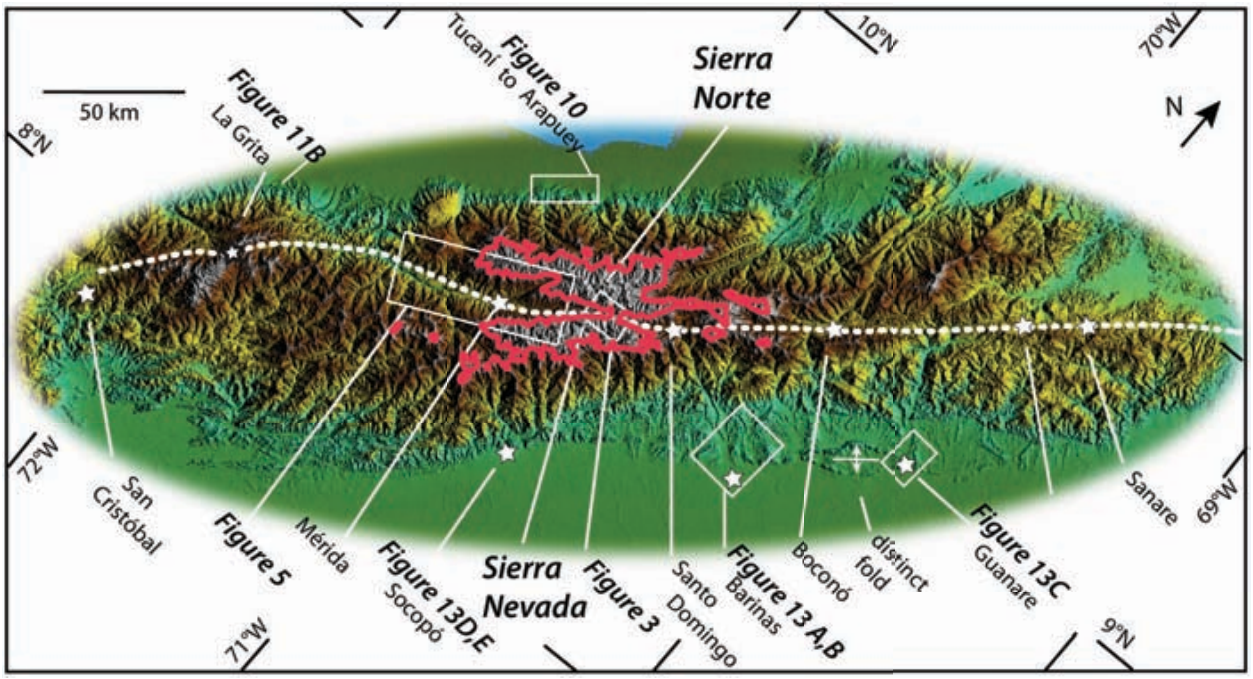

852

853 Fig. 2. Physiographic map of Venezuelan Andes shows location of Boconó fault (thick dashed
854 line) and locations of cities (stars) and figures (white boxes and annotations) cited in text. The
855 3500-m contour interval (gray–red) approximates estimates of the ice extent during the Last
856 Glacial Maximum (e.g., Schubert, 1974; Stansell et al., 2007b).

857

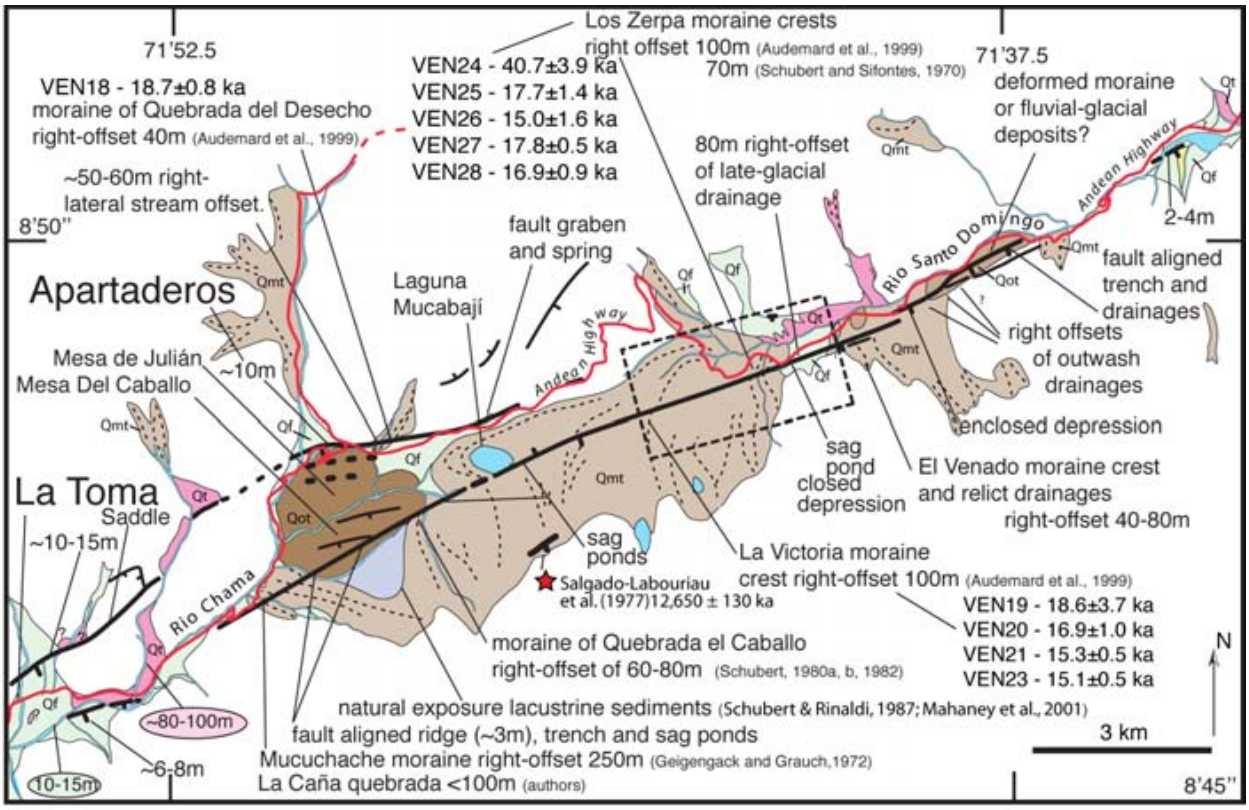

858

859 Fig. 3. Quaternary deposits, traces of the Boconó fault, previously reported measured offsets of
860 moraines, scarp height measurements of authors, and surface exposure ages for boulders on the
861 La Victoria and Los Zerpa moraines. (Location of this map outlined in Fig. 2.) Small dashed box
862 is footprint of aerial photograph shown in Fig. 4. In order of decreasing relative age, unit Qot is
863 older glacial till, Qmt is late Pleistocene moraines and till deposits of the latest glacial period, Qt
864 is valley fill terrace deposits (unit Qt), and Qf is late Pleistocene and Holocene alluvial fan
865 deposits. Moraine crests marked by dashed lines. Star shows location of radiocarbon sample site
866 of Salgado-Labouriau et al. (1977). Values in ovals are measures of stream incision. Laguna
867 Mucabají sits within drainage divide between Ríos Chama and Santo Domingo.

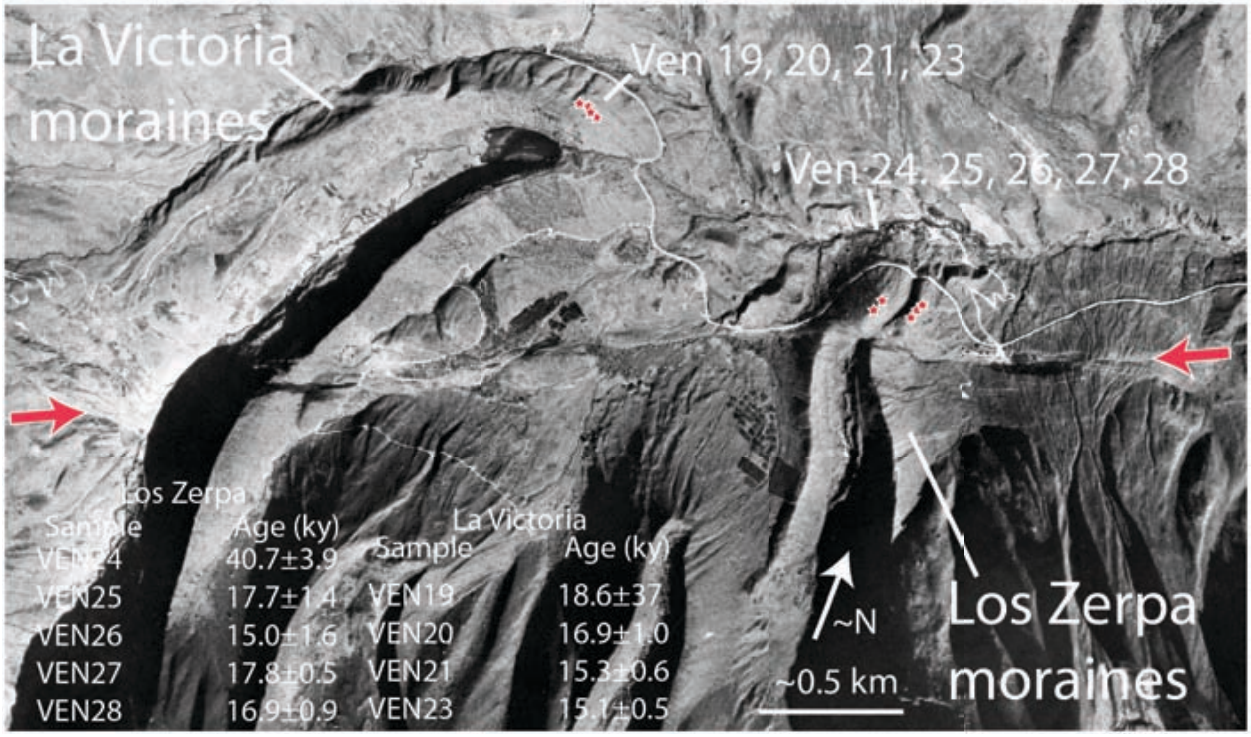

Fig. 4. The Boconó fault trace (along strike between arrows) produces opposite-facing scarps, sag ponds, and offsets of the La Victoria and Los Zerpa moraine crests first observed by Cluff and Hansen (1969) and Schubert and Sifontes (1970). Locations (stars) and ages (text at lower left, also in Table 1) of boulder samples collected and subject to ^{10}Be cosmogenic analysis are annotated. Location of moraines is shown in Fig 3.

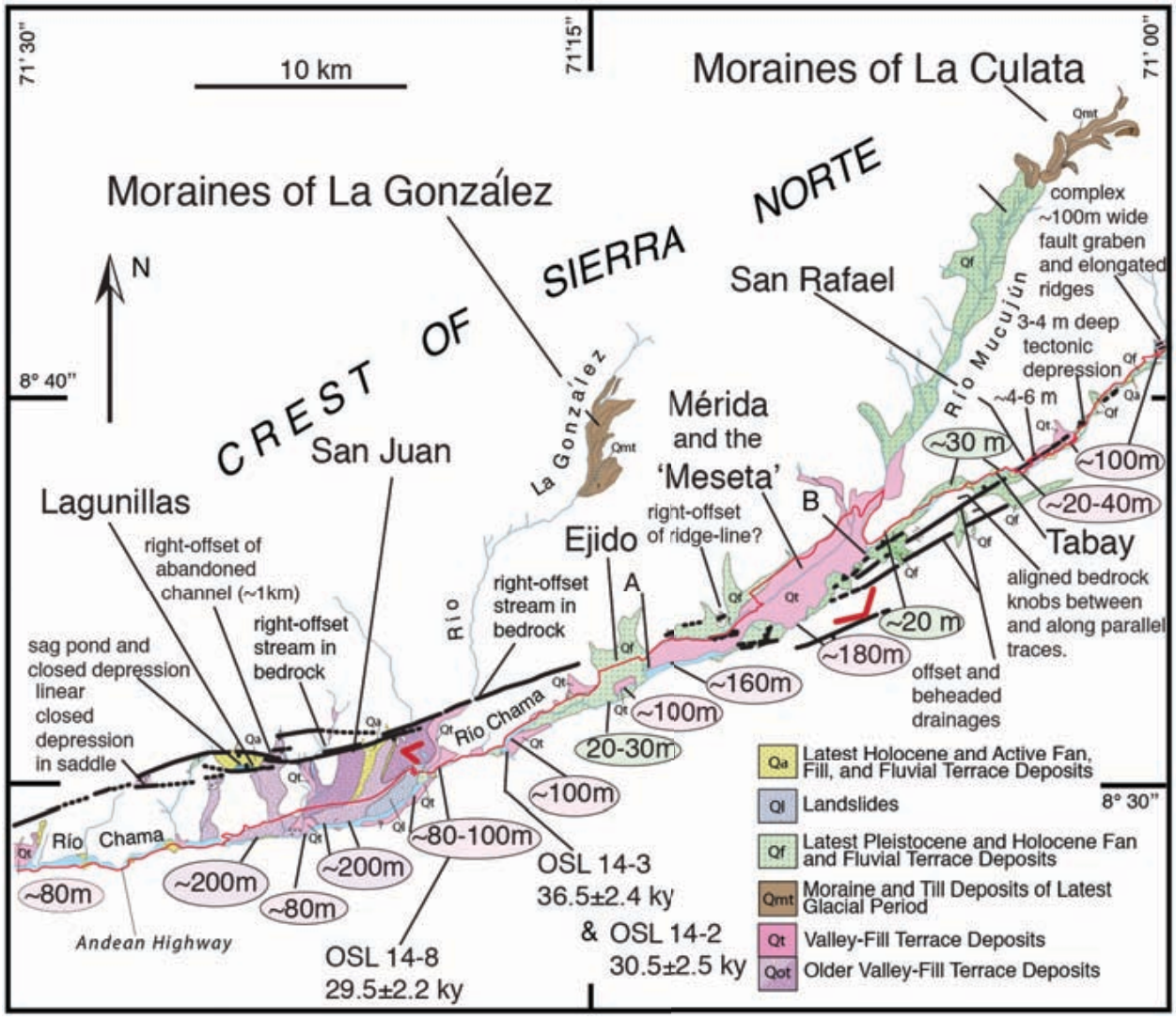

874

875 Fig. 5. Quaternary deposits along the Ríos Chama and Mucujún and traces of the Boconó fault
876 (thick black lines). Annotations further indicate locations of OSL samples analyzed, field
877 measurements of amount of incision of Quaternary terrace surfaces along the Río Chama (values
878 in ellipses), and tectonic geomorphology illustrating the active nature of the Boconó fault.
879 Outwash associated with the moraines of La González and La Culata filled the valley and now is
880 recorded by terrace deposits (unit Qt) along the Río Chama. Values in ellipses are amounts of
881 incision of fill deposits by the Río Chama. Another trace of the Boconó may be hidden by the
882 course of the Río Chama southwest of Ejido as well (Schubert, 1982). Small V-forms show
883 perspective of photos in Figs. 7 and 9, respectively. Points A and B are the limits of the survey
884 shown in Fig. 8.

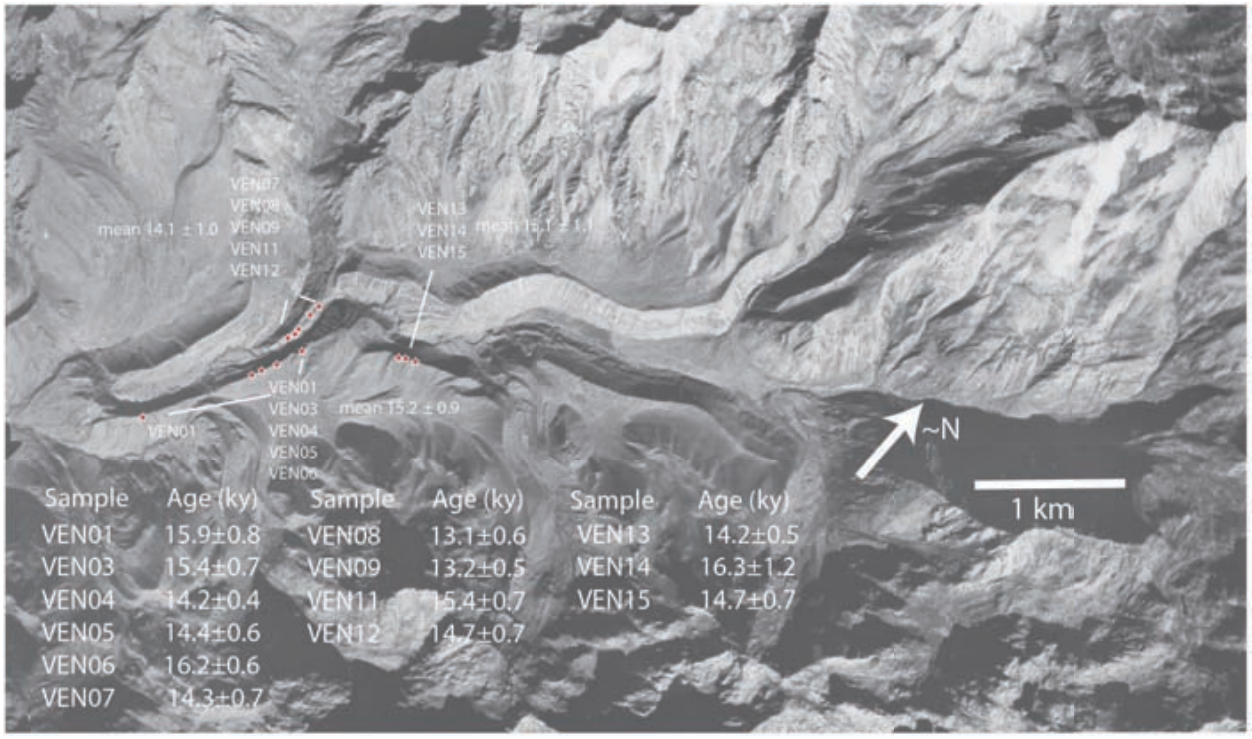

Fig. 6. Aerial photograph of the moraines of La Culata shows location of boulders sampled for cosmogenic analysis (small stars). Samples VEN01 through 07 and VEN13 through 15 are from the crests of major laterofrontal moraines, and samples VEN07 through VEN12 from a lesser inset laterofrontal moraine. Ages of individual samples are annotated. Location of moraines are shown on map of Figure 5.

Fig. 7. View northward across the Río Chama to the meseta on which the city of Mérida rests. Perspective of photo is shown by V symbol near Merida in Fig. 5. The meseta is interpreted to be largely composed of glacial outwash deposits transported down the Río Mucujún and into the Río Chama. Ages from OSL dating suggest that the deposits were largely emplaced ~ 30 and 37 ka.

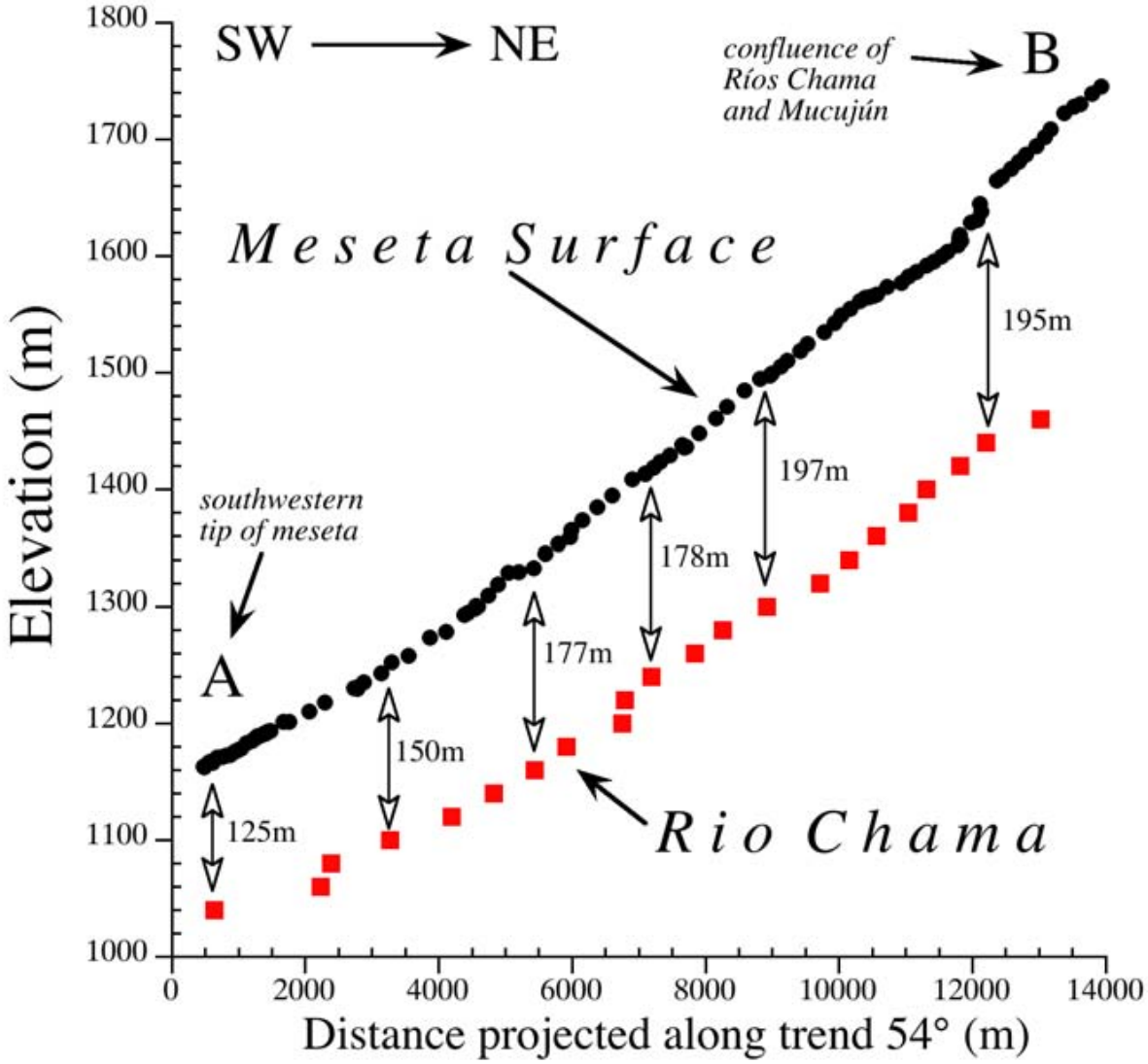

900

901 Fig. 8. Survey of elevations along the edge of the meseta surface (solid circles) and the Río
902 Chama (solid squared) projected along azimuth of 54° shows that thickness of sediments on
903 which the meseta is constructed increases upstream from the tip of the meseta to the confluence
904 of the Rios Chama and Mucujún. Endpoints A and B annotated on Figure 5.

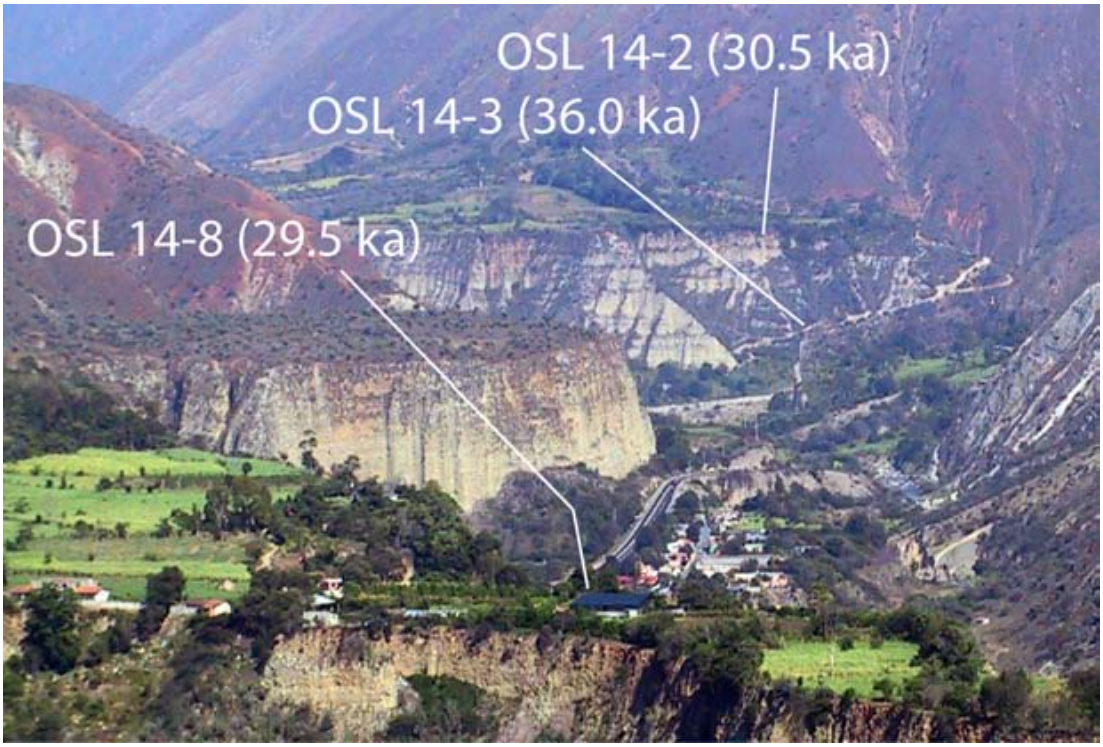

Fig. 9. View northeastward along Río Chama showing characteristics of remnant glacial outwash deposits that once filled the valley. Locations and ages of OSL samples are annotated here and also on the map of Fig. 5. Perspective of view is also shown by red V symbol near San Juan in Fig. 5.

Fig. 10. Fault-truncated alluvial surfaces along northwestern flank of Andes are labeled 1, 2, 3, and 4 (values in circles) and, respectively, exhibit scarp heights of 3-5, ~10, ~20, and 120 m and record progressive late Quaternary uplift. Names, ages, and locations of boulders sampled for ^{10}Be TCN analysis near Tucaní are labeled. Scarp height measurements in meters. Photograph of 3-m-high scarp east of Arapuey is shown in Fig. 11A. Limits of profile measurements at Tucaní (stars) that are shown in Fig. 12 are labeled AB and EF, respectively. Lago de Maracaibo is at sea level and the contours outboard of the Andes are at 10-m intervals. Red line is Carretera Panamericana (highway). Bedrock in the Andes (stippled) and unfaulted alluvium outboard (northwest) of rangefront are undifferentiated.

Fig. 11. Examples of youthful fault scarps along the northwestern flank of the Andes. (A) Scarp of ~ 3 m height at Arapuey as viewed northeastward from where it crosses the Carretera Panamericana (highway). Site is located at 9°15'53.5" N, 70°55'57.8" W. Location also noted in Fig. 10. (B) Scarp preserved across small embayment along rangefront between pueblos of La Blanca and Morotuto. Location of site is 8°23'27.2" N, 72°01'20.0" W and location also annotated on Fig. 2. White dotted lines drawn along the base of each scarp.

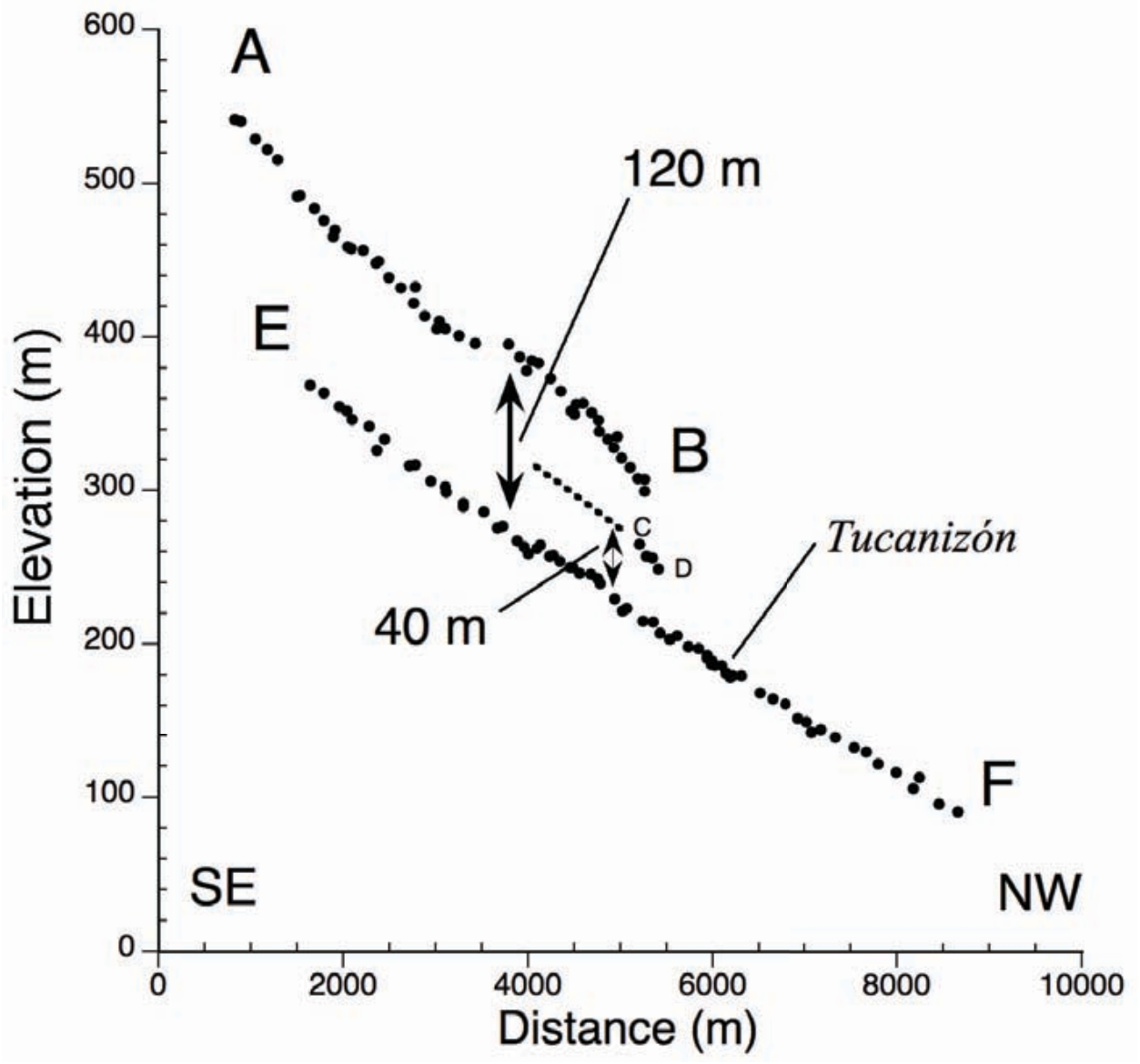

931

932 Fig. 12. Survey of fault-truncated and abandoned fan surface at Tucaní. Survey lines AB and EF
933 are annotated on map in Fig. 10. Line AB is along the highest surface. Line EF is along the
934 current river grade. Line CD is on the surface intermediate in elevation between river grade and
935 the high terrace. Elevation of the highest terrace surface above stream grade is ~ 120 m.

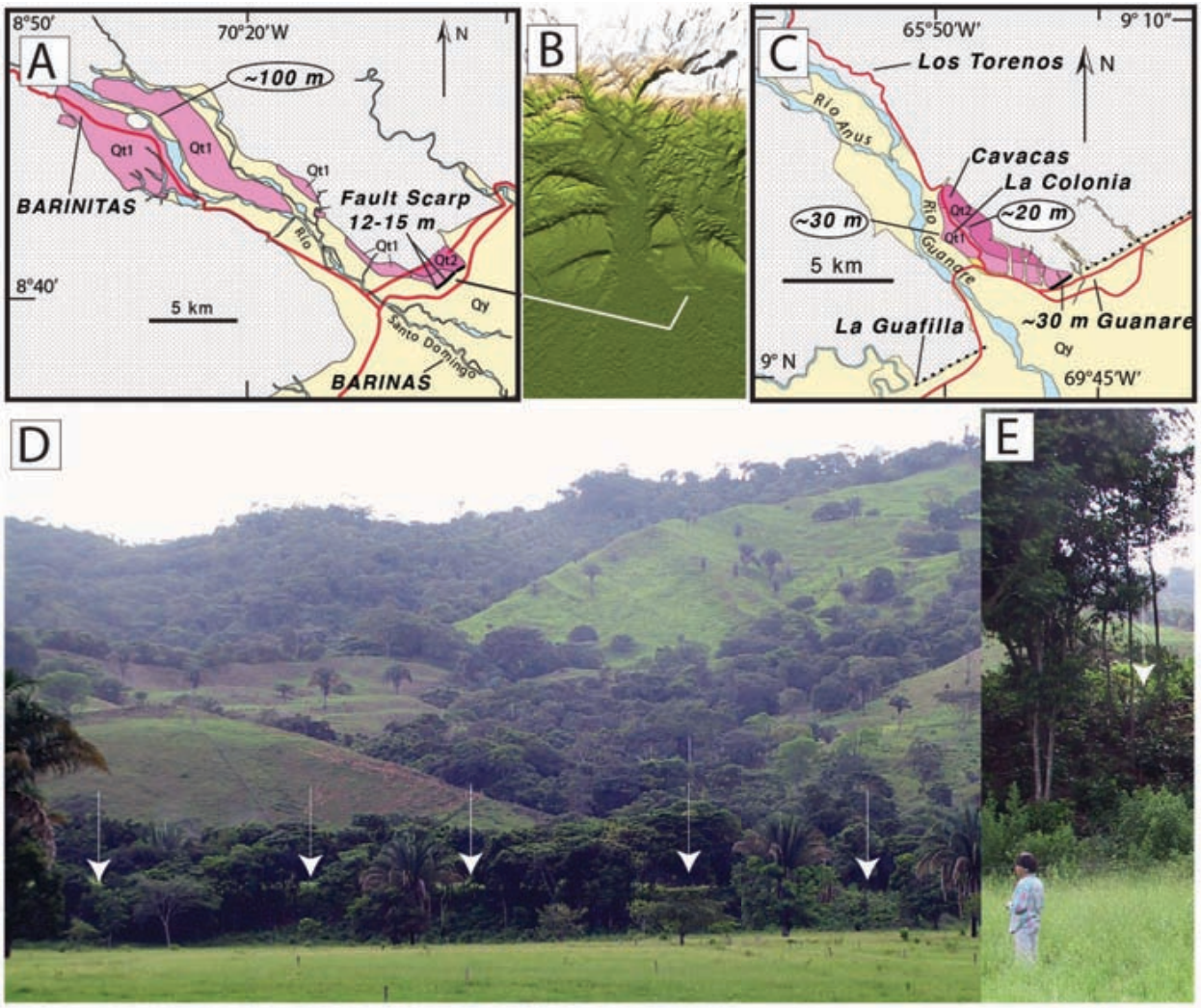

Fig. 13. Observations showing recent and ongoing Quaternary uplift along the southeastern flank of the Andes caused by a bounding thrust fault (dark solid lines in maps) that emerges to or very near the surface. (Upper) Pleistocene strath terrace surfaces truncated at and near the southwestern Andean rangefront near Barinas (A) and Guanare (C) are shaded and labeled Qt1 and Qt2, respectively. An SRTM image (C) of the Barinas region shown in (A). (lower) Example of young fault scarp in alluvial apron near Socopó (D) is also shown in closer view in (E). White arrows in (D) and (E) point to crest of scarp highlighted in sunlight. Fault scarp heights are annotated. Locations and magnitudes of incision of terrace and older terrace risers are shown by pointer and values in ovals. Site locations are annotated in Fig. 2.

Table 1

Locations for ^{10}Be TCN samples, sample sizes, topographic shielding factors, concentrations, and analytical results and ages.

Sample number and location name	Lithology	Location latitude (°N)	Location longitude (°W)	Elevation (m asl)	Size[a] a/b/c axes (cm)	Thickness (cm)	Production rate (atoms/g/y) Spallation[b]	Production rate (atoms/g/y) Muons[c]	Shielding factor	Quartz[d] (g)	Be carrier[e] (mg)	^{10}Be/^{9}Be[f,g] (x 10^{-15})	^{10}Be concentration[g,h,i] (x 10^{3} atoms/g SiO_2)	Age[i,j,k,l] Lal (1991)/Stone (2000) time independent (ka)
La Culata llgm moraines														
VEN1	Metagranite	8.7601	71.0516	3391	230/190/140	5	23.43	0.50	1	12.1261	0.3531	137±7	378±18	15.9±0.8 (1.6)
VEN3	Metagranite	8.7654	71.0477	3457	330/300/175	3	24.64	0.52	1	15.3985	0.3501	179±8	386±16	15.4±0.7 (1.5)
VEN4	Metagranite	8.7656	71.0476	3458	190/150/90	3	24.65	0.52	1	22.1585	0.3526	236±6	355±9	14.2±0.4 (1.3)
VEN5	Metagranite	8.7663	71.0471	3467	280/220/100	4	24.56	0.51	1	16.7894	0.3553	180±8	360±16	14.4±0.6 (1.4)
VEN6	Metagranite	8.7689	71.0457	3508	250/210/75	2	25.50	0.53	1	15.1772	0.3565	189±7	420±16	16.2±0.6 (1.6)
													Average	**15.2±0.9**
La Culata younger inset moraine														
VEN7	Metagranite	8.7697	71.0467	3472	220/180/100	3	24.43	0.52	0.980	15.2250	0.3531	162±8	354±17	14.3±0.7 (1.4)
VEN8	Metagranite	8.7697	71.0466	3472	120/100/70	4	24.12	0.52	0.980	8.3870	0.3508	81±4	321±15	13.1±0.6 (1.3)
VEN9	Metagranite	8.7705	71.0466	3477	180/160/110	3	24.40	0.52	0.980	18.4711	0.3498	183±7	327±13	13.2±0.5 (1.3)
VEN11	Metagranite	8.7721	71.0464	3501	220/100/70	5	24.23	0.52	0.978	17.9667	0.3531	205±9	380±17	15.4±0.7 (1.5)
VEN12	Granite	8.7726	71.0463	3500	160/70/70	2	24.81	0.52	0.977	19.8966	0.3508	223±11	372±18	14.7±0.7 (1.5)
													Average	**14.2±1.0**
La Culata llgm moraines														
VEN13	Metagranite	8.7729	71.0393	3657	530/260/350	5	26.79	0.54	1	8.0315	0.3502	93±3	386±14	14.2±0.5 (1.3)
VEN14	Granite	8.7729	71.0395	3653	235/150/70	4	27.07	0.54	1	15.0289	0.3509	203±15	448±33	16.3±1.2 (1.9)
VEN15	Granite	8.7727	71.0400	3651	230/130/150	4	26.93	0.54	1	16.5257	0.3505	200±10	402±20	14.7±0.7 (1.5)
													Average	**15.1±1.1**
llgm faulted moriane														
VEN18[m]	Granite	8.8043	70.8417	3651	250/140/45	3	27.04	0.54	0.991	17.9456	0.3533	276±12	513±23	18.7±0.8 (1.8)
La Victoria llgm moraine														
VEN19	Gniess	8.8141	70.8006	3255	180/130/80	2	22.40	0.49	1	15.0044	0.3522	191±38	423±84	18.6±3.7 (4.1)
VEN20	Gniess	8.8142	70.8006	3258	280/150/40	3	22.25	0.49	1	15.2109	0.3501	177±10	382±21	16.9±1.0 (1.8)
VEN21	Gniess	8.8142	70.8010	3260	190/90/55	2	22.46	0.49	1	16.3238	0.3536	170±7	349±14	15.3±0.6 (1.5)
VEN23	Metagranite	8.8139	70.7993	3243	120/110/40	2	22.26	0.49	1	19.9312	0.3496	207±6	343±11	15.1±0.5 (1.4)
													Average	**16.5±1.6**
Las Zerpas faulted llgm moraine														
VEN24	Gneiss	8.8117	70.7883	3128	320/200/90	2	20.95	0.47	1	18.4540	0.3500	481±46	863±82	40.7±3.9 (5.3)
VEN25	Gneiss	8.8121	70.7881	3115	350/230/150	2	20.80	0.47	1	15.5746	0.3497	177±14	375±29	17.7±1.4 (2.1)
VEN26	Gneiss	8.8120	70.7873	3104	180/150/75	3	20.95	0.47	1	22.9746	0.3537	216±22	315±32	15.0±1.6 (2.0)
VEN27	Gneiss	8.8117	70.7875	3105	250/230/100	3	20.52	0.47	1	21.6626	0.3510	241±7	370±11	17.8±0.5 (1.6)
VEN28	Gneiss	8.8118	70.7873	3106	110/90/40	2	20.79	0.47	1	20.5055	0.3537	220±11	358±18	16.9±0.9 (1.7)
													Average[n]	**16.9±1.3**
Rio Tucanizon alluvial fans/terrace surfaces														
VEN29	Granite	8.9503	71.2407	442	120/60/40	3	3.66	0.21	1	16.2095	0.3517	81±7	167±15	43.6±4.0 (5.5)
VEN30	Granite	8.9505	71.2405	440	170/160/75	3	3.67	0.21	1	15.8490	0.3512	238±33	500±69	133.0±19.0 (22.5)
VEN31	Metasandstone	8.9505	71.2405	436	120/120/65	2	3.69	0.21	1	15.3295	0.3526	129±6	280±13	73.1±3.4 (7.3)
VEN32	Metasandstone	8.9565	71.2695	340	450/280/270	4	3.37	0.20	1	15.0303	0.3510	202±7	447±16	129.1±4.8 (12.5)
VEN33	Metasandstone	8.9511	71.2666	381	190/120/70	3	3.50	0.21	1	15.7633	0.3505	139±6	293±13	80.5±3.7 (8.0)
VEN34	Metasandstone	8.9509	71.2666	384	120/60/45	4	3.48	0.21	1	10.4128	0.3535	69±3	221±10	60.9±2.9 (6.1)
													Range	**44-133**

[a]Diameter of boulders: a=maximum length, b=maximum width, and c=maximum height.

[b]Constant (time-invariant) local production rate based on Lal (1991) and Stone (2000). A sea level, high latitude value of 4.5 ± 0.3 at ^{10}Be g^{-1} quartz was used.

[c]Constant (time-invariant) local production rate based on Heisinger et al. (2002a,b).

[d]A density of 2.7 g cm^{-3} was used for all surface samples.

[e]Concentration of carrier = 1.414 ppm.

[f]Isotope ratios were normalized to ^{10}Be standards prepared by Nishiizumi et al. (2007) with a value of 2.85 x 10^{-12} and using a ^{10}Be half life of 1.36 x 10^{6} years.

[g]Uncertainties are reported at the 1σ confidence level.

[h]Samples were corrected for a mean blank ^{10}Be/^{9}Be = 2.27 ± 1.04 x 10^{-15}.

[i]Propagated uncertainities include error in the blank, carrier mass (1%), and counting statistics.

[j]Propagated error in the model ages include a 6% uncertainty in the production rate of ^{10}Be and a 4% uncertainty in the ^{10}Be decay constant.

[k]Beryllium-10 model ages were calculated with the CRONUS-Earth online calculator, version 2.2 (Balco et al., 2008; http://hess.ess.washington.edu/).

[l]Constant (time-invariant) local production rate based on Lal (1991) and Stone (2000). The uncertainty quoted is analytical, whereas uncertainty in parenthesis is the external uncertainty that includes analytical and production rate uncertainty.

[n]Sample VEN18 was collected from a faulted moraine. However, we were not able to attract quartz from other samples collected from this moraine. We include it in this table for reference for future workers, but do not discussed in our manuscript.

[m]Sample VEN24 was not considered in the average because its date is many standard deviations outside of the cluster of ages on this moraine. It is likely this boulder contains inherited TCNs.

Table 2
Summary of OSL dating results from quartz extracted from sediment sample: particle size, sample locations, radioisotope concentrations, cosmic dose rates, total dose-rates, D_E values, and optical ages.

Sample number	Particle size (μm)	Location (N/W)	Altitude (m a.s.l.)	Depth (cm)	U[a] (ppm)	Th[a] (ppm)	K[a] (%)	Rb[a] (ppm)	Cosmic dose rate[b] ($mGya^{-1}$)	Total dose-rate[c,d] ($mGya^{-1}$)	Number of aliquots[e]	Mean D_E[f] (Gy)	Age (ka)
14-2	90-125	8.5°/ 71.3°	938	500	3.06	10.9	2.23	112	0.13±0.01	3.42±0.21	22(16)	104.4±5.7	30.5±2.5
14-3	90-125	8.5°/ 71.3°	880	5800	4.76	13.3	2.11	108	0.03±0.003	3.74±0.22	18(15)	134.5±5.9	36.0±2.4
14-8	90-125	8.5°/ 71.3°	859	500	3.24	14.9	2.26	117	0.13±0.01	3.74±0.22	17(16)	110.6±5.1	29.5±2.2

[a]Elemental concentrations from NAA of whole sediment measured at USGS Nuclear Reactor in Denver. Uncertainty taken as ±10%.
[b] Estimated contribution to dose-rate from cosmic rays calculated according to Prescott and Hutton (1994). Uncertainty taken as ±10%.
[c] Estimated fractional water content from whole sediment is 10 ± 5%.
[d]Total dose-rate from beta, gamma, and cosmic components. Beta attenuation factors for U, Th, and K compositions incorporating grain size factors from Mejdahl (1979). Beta attenuation factor for Rb arbitrarily taken as 0.75 (cf. Adamiec and Aitken, 1998). Factors utilized to convert elemental concentrations to beta and gamma dose rates from Adamiec and Aitken (1998) and beta and gamma components attenuated for moisture content.
[e] Number of aliquots measured. The number in parentheses refers to the number of aliquots used to calculate the D_E.
[f]Mean equivalent dose (D_E) determined from replicated single-aliquot regenerative-dose (SAR; Murray and Wintle, 2000) runs. Errors are 1 σ standard errors (i.e. $\sigma_{n-1}/n^{1/2}$) incorporating error from beta source estimated at about ±5%.